# Metabolic evolution and the self-organization of ecosystems

Rogier Braakman[a,b,1], Michael J. Follows[b], and Sallie W. Chisholm[a,c,1]

[a]Department of Civil and Environmental Engineering, Massachusetts Institute of Technology, Cambridge, MA 02139; [b]Department of Earth, Atmospheric, and Planetary Sciences, Massachusetts Institute of Technology, Cambridge, MA 02139; and [c]Department of Biology, Massachusetts Institute of Technology, Cambridge, MA 02139

Contributed by Sallie W. Chisholm, February 22, 2017 (sent for review November 28, 2016; reviewed by Ron Milo and John A. Raven)

**Metabolism mediates the flow of matter and energy through the biosphere. We examined how metabolic evolution shapes ecosystems by reconstructing it in the globally abundant oceanic phytoplankter *Prochlorococcus*. To understand what drove observed evolutionary patterns, we interpreted them in the context of its population dynamics, growth rate, and light adaptation, and the size and macromolecular and elemental composition of cells. This multilevel view suggests that, over the course of evolution, there was a steady increase in *Prochlorococcus*' metabolic rate and excretion of organic carbon. We derived a mathematical framework that suggests these adaptations lower the minimal subsistence nutrient concentration of cells, which results in a drawdown of nutrients in oceanic surface waters. This, in turn, increases total ecosystem biomass and promotes the coevolution of all cells in the ecosystem. Additional reconstructions suggest that *Prochlorococcus* and the dominant cooccurring heterotrophic bacterium SAR11 form a coevolved mutualism that maximizes their collective metabolic rate by recycling organic carbon through complementary excretion and uptake pathways. Moreover, the metabolic codependencies of *Prochlorococcus* and SAR11 are highly similar to those of chloroplasts and mitochondria within plant cells. These observations lead us to propose a general theory relating metabolic evolution to the self-amplification and self-organization of the biosphere. We discuss the implications of this framework for the evolution of Earth's biogeochemical cycles and the rise of atmospheric oxygen.**

metabolic evolution | *Prochlorococcus* | microbial oceanography | mutualism | Earth history

Metabolism sustains the nonequilibrium chemical order of the biosphere by continually supplying the energy and building blocks of all cells on Earth (1–5). Here we ask: How does cellular metabolic evolution shape the mass and energy flows of ecosystems? The oceanic phytoplankter *Prochlorococcus* (6), the most abundant photosynthetic cell on Earth (7, 8), provides an ideal model system for addressing this question. *Prochlorococcus* and its deeper-branching sister lineage marine *Synechococcus* make up the marine picocyanobacteria and have a characteristic biogeography (9). *Prochlorococcus* "ecotypes" have geographically (10, 11) and seasonally (12) dynamic populations that in warm, stable stratified water columns always return to the same general structure: Recently diverging high-light-adapted (HL) ecotypes are most abundant toward the surface, whereas deeper branching low-light-adapted (LL) ecotypes are most abundant at depth (10–14) (Fig. 1).

What selective forces drove this niche partitioning in *Prochlorococcus*, and what were the consequences for the ocean ecosystem in general? To address these questions, we reconstructed (15, 16) (Fig. 2) the evolution of core metabolism in strains representing the major clades of *Prochlorococcus*. To interpret the observed patterns, we developed an evolutionary framework that illuminates the driving forces that produced many of the features of *Prochlorococcus*. Using this framework, we argue that the evolutionary patterns manifested in the *Prochlorococcus* collective reflect fundamental processes shaping the coevolution of the chemistry of the oligotrophic oceans and the microbial ecosystems they harbor.

## Results and Discussion

**Metabolism Provides Clues About Large-Scale Evolutionary Driving Forces.** To examine the driving forces shaping the evolution of *Prochlorococcus*, we reconstructed (Fig. 2) the evolution of its metabolic core (*SI Appendix*, Fig. S1). Because all biosynthetic pathways originate there, its evolution is highly constrained, and any innovations likely reflect major driving forces (5). Previous studies identified some unique presence/absence patterns for core metabolic genes in both *Prochlorococcus* and *Synechococcus* and relative to other cyanobacteria. For example, both have replaced the cyanobacterial RuBisCO and related proteins of the $CO_2$-concentrating mechanism with proteobacterial variants (17–19), lost key genes in the cyanobacterial TCA cycle (20) and glycolysis (21), and acquired a menaquinone-based malate dehydrogenase (22). Photorespiration proteins are, in turn, universally preserved in *Synechococcus*, but unevenly distributed across *Prochlorococcus* ecotypes (9, 23).

Expanding on these studies, we surveyed cyanobacteria for the presence/absence of core metabolic genes (*SI Appendix*, Table S1 and Fig. S1) and mapped this distribution onto their phylogeny to reconstruct a phylometabolic tree (Fig. 2) that resolves the evolution of *Synechococcus* and *Prochlorococcus* (Fig. 1). All of the variations are part of a sequence of innovations that remodeled the metabolic core as *Prochlorococcus* diverged from the rest of cyanobacteria (Fig. 3). Key innovations occur in ancestral freshwater lineages (Fig. 3 and *SI Appendix*, Table S1), indicating that underlying selection pressures preceded the emergence of the marine lineages.

### Significance

**Understanding what drives self-organization in complex systems and how it arises is a major challenge. We addressed this challenge using dominant oceanic photosynthetic and heterotrophic microbes as a model system. Reconstructing the metabolic evolution of this system suggests that its self-organization and self-amplification were coupled and driven by an increasing cellular energy flux. Specifically, the evolution of cells steadily increased their metabolic rate and excretion of organic carbon. We describe how this increases cellular nutrient uptake and thereby ecosystem biomass. The release of organic carbon, in turn, promotes positive feedbacks among species that reinforce this evolutionary drive at the ecosystem level. We propose the evolutionary self-organization of oceanic microbial ecosystems contributed to the oxygenation of Earth.**

Author contributions: R.B. designed research; R.B. performed research; R.B. contributed new reagents/analytic tools; R.B. developed the model; M.J.F. contributed to model development; R.B. and S.W.C. analyzed data; and R.B., M.J.F., and S.W.C. wrote the paper.

Reviewers: R.M., Weizmann Institute; and J.A.R., University of Dundee, U.K.

The authors declare no conflict of interest.

Freely available online through the PNAS open access option.

[1]To whom correspondence may be addressed. Email: rogierbraakman@gmail.com or chisholm@mit.edu.

This article contains supporting information online at www.pnas.org/lookup/suppl/doi:10.1073/pnas.1619573114/-/DCSupplemental.

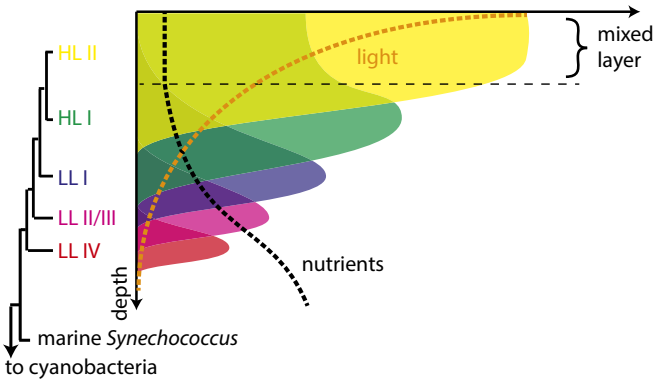


**Fig. 1.** Typical relative abundance distributions of *Prochlorococcus* ecotypes as a function of depth and accompanying light intensity and nutrient concentration profiles in stratified oceanic waters. Ecotype populations are geographically and temporally dynamic, but in warm, stable water columns return to this same depth-differentiated state (12). The deepest branching ecotypes are most abundant at the bottom of the euphotic zone, where nutrient concentrations are high and light energy low. The most recently diverging ecotypes are most abundant near the surface, where the reverse is true (10–14). HL, high-light-adapted; LL, low-light-adapted.

The remodeling of *Prochlorococcus*' metabolic core includes the disruption of photorespiration and the TCA cycle (Fig. 3 and *SI Appendix*, Fig. S1), raising the possibility that intermediates of truncated pathways are excreted from the cell. Phytoplankton commonly excrete organic carbon as an outlet of excess reducing power under nutrient limitation or intense light (24). Analogously, when facing a large energy supply from organic carbon, some heterotrophs will effectively drain reducing power into the environment by excreting partially oxidized organic carbon rather than fully oxidizing it to $CO_2$ (25–28), whereas some photoheterotrophs use $CO_2$-fixation as a sink for excess reducing power (29). For photosynthetic cells in the oligotrophic surface oceans, where the solar energy supply may commonly outpace the nutrient supply (Fig. 1), the combination of increased $CO_2$ fixation and increased excretion of organic carbon could thus well be under strong selection. This is consistent with observations that *Prochlorococcus* has the most efficient carbon-concentrating mechanism (30) and highest known rate of $CO_2$ fixation per photosynthetic pigment (31) of any phytoplankton, even though its small size and slow growth (6, 32) suggest a relatively small carbon flux requirement. Lastly, selection to rid the system of excess reducing power is consistent with the acquisition of the Plastoquinol Terminal Oxidase (PTOX) in the LLI and HL clades of *Prochlorococcus* (Fig. 3 and *SI Appendix*, Table S1), which adds an additional outlet for excess reducing power in their photosynthetic electron transfer chain (*SI Appendix*, Fig. S1) (33–36).

That the evolution of *Prochlorococcus* permanently increased the excretion of organic carbon in its late-branching strains is also consistent with limited laboratory observations. At moderate light levels in nutrient replete medium, strains from HL clades that dominate surface waters (Fig. 1) excrete up to 20% of fixed carbon, and recently diverging strains excrete the most (37). Cells excrete significant amounts of glycolate (37), one of the dead ends in the metabolic network (*SI Appendix*, Fig. S1). P-starved cells excrete slightly less carbon (37), but this could be due to the coincident cessation of growth. Nevertheless, a higher fraction of the carbon excreted by P-starved cells consists of glycolate and other small carboxylic acids (37). Many phytoplankton excrete glycolate under intense light or nutrient limitation (24, 38), but retain the capacity to recycle it by using the three-subunit iron–sulfur protein glycolate oxidase (GlcDEF, rxn 13 in *SI Appendix*, Fig. S1), shown to be the enzymatic workhorse for this function in cyanobacteria (23). However, this gene is absent in all but the deepest-branching LLIV clade of *Prochlorococcus* (*SI Appendix*, Table S1), suggesting a permanent opening of this pathway early in its evolution (Fig. 3). Finally, the bulk of organic carbon excreted by *Synechococcus* consists of polysaccharides (39), which are commonly excreted by nutrient-limited microbes (26, 40), suggesting that these compounds could similarly act as a redox safety valve in *Prochlorococcus*, which dominates in one of the most nutrient-poor environments on Earth (7–9) (Fig. 1).

We further examined the possibility that the evolution of *Prochlorococcus* increased its excretion of organic carbon as an outlet of excess reducing power (Fig. 3) through additional genomic analyses. Functionally related and coexpressed genes are commonly located near each other, so we searched the genomic neighborhoods of core metabolic genes for transporters across clades (*SI Appendix*, Fig. S2). We identified chromosome rearrangements repositioning a series of transporters, including three export and one import transporters, near key metabolic genes, consistent with selection acting to fortify the control of transport pathways (*SI Appendix*, Fig. S2). Chromosome rearrangements are seen in freshwater picocyanobacteria (*SI Appendix*, Fig. S2), again suggesting that these pathways came under selection before the emergence of the marine lineages and the loss of photorespiration in the LLII/III clade of *Prochlorococcus* (Fig. 3 and *SI Appendix*, Fig. S1). This analysis suggests that, in addition to glycolate, pyruvate and citrate (or isocitrate) are exported, whereas malate is imported (*SI Appendix*, Figs. S1 and S2).

Furthermore, because environmentally driven variations in the expression of genes can give insight into their function [i.e., "reverse ecology" (41)], and the metabolism of *Prochlorococcus* is highly choreographed to the diel light:dark cycle (42, 43), we examined the gene expression of a HL-adapted strain grown under a diel cycle (42). All putative export pathway genes have mRNA expression maxima at sunrise (*SI Appendix*, Fig. S2), consistent with their acting as redox safety valves, activated when the supply of reducing power increases at dawn. Similarly,

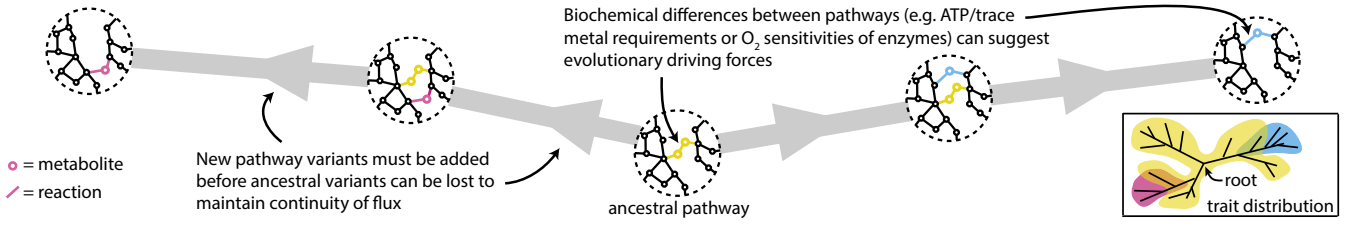


**Fig. 2.** Illustration of approach to metabolic reconstructions. Phylometabolic trees reflect the evolution of metabolic network phenotypes because they integrate constraints from phylogenetics and metabolism (15, 16). All sequenced genomes within a given clade are searched for the presence/absence of enzymes catalyzing the reactions of different pathways. Mapping pathway variability patterns onto phylogenies of the clade suggests the order of metabolic innovations. In this example, three alternative pathways (pink, yellow, and blue) connect essential and universal pathways (black). Genes for the yellow pathway are nearly universally distributed (*Inset*), suggesting that it is the ancestral pathway, with the pink and blue pathways deriving from it. Maintaining continuity of flux results in trees of functional phenotypes. Biochemical differences between alternative pathways (e.g., ATP/trace metal requirements or oxygen sensitivities of their enzymes) suggest evolutionary driving forces (15, 16).

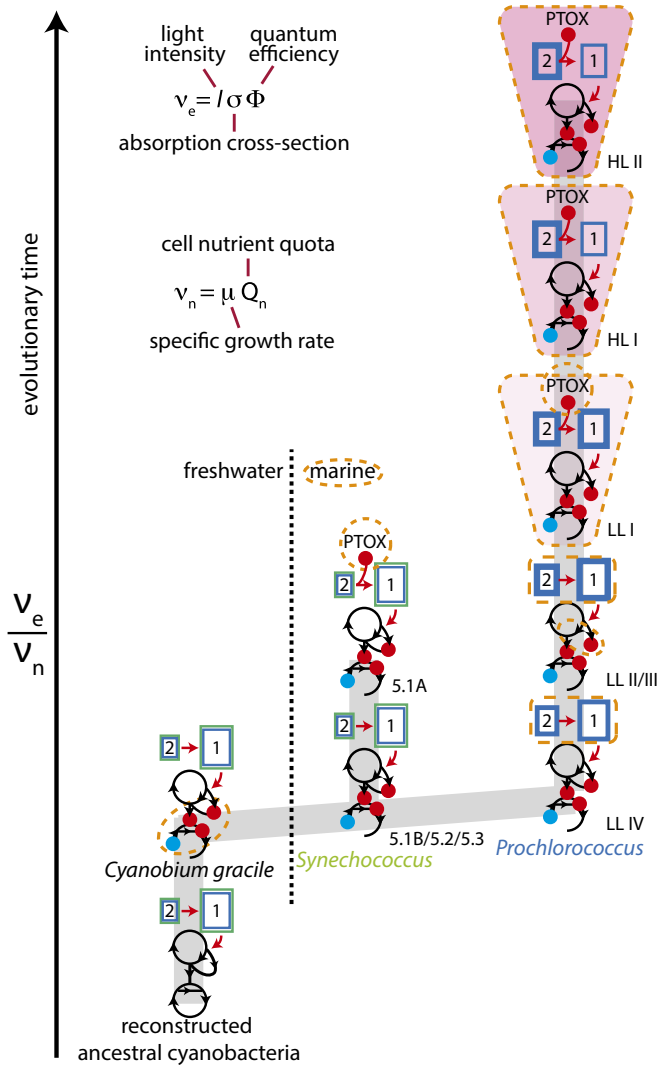


**Fig. 3.** Metabolic evolution of *Prochlorococcus*. The metabolic variants are represented in simplified form along a gradient of the ratio of electron flux to nutrient flux $\nu_e/\nu_n$. Innovations (*SI Appendix*, Fig. S1 and Table S1) are highlighted with dashed orange lines. Cellular electron drains are represented as red dots and uptake pathways as blue dots. Photosystems are represented as boxed 2's and 1's, and their colors reflect the major absorption wavelengths, their line thickness reflects their absorption cross-section, and their relative size reflects the PSII:PSI ratio (*SI Appendix*, Fig. S1). Key innovations in the HLI and HLII clades are related to protection/repair of direct photodamage (52, 53), including UV damage, as indicated by a darkening protective pink shade.

the expression of PTOX, the most immediate outlet for excess reducing power in the electron transfer chain (*SI Appendix*, Fig. S1), is maximal at midday (35, 42). Collective evidence thus suggests that the evolution of *Prochlorococcus* steadily added redox outlets, leading to increased excretion of organic carbon. Lastly, expression of the putative malate uptake pathway peaks at dusk (*SI Appendix*, Fig. S2), suggesting that the rest of the ecosystem may return some organic carbon to *Prochlorococcus* at night.

What drove *Prochlorococcus*' increased excretion of organics over the course of its evolution? If maintaining redox balance was the driving force, why not enhance the ability to lower photosynthetic electron flux (44, 45), which many photosynthesizers use to prevent redox imbalance (46, 47)? Because *Prochlorococcus* carries out a sizable fraction of the primary production in these ecosystems, perhaps metabolic interdependencies with cooccurring heterotrophs are in play. Invoking cross-feeding interactions to explain excretion of organic carbon by *Prochlorococcus* is problematic, however, because in unstructured populations typical of oceanic microbes, the apparent cost of fixing and excreting carbon leads to a "public goods" dilemma: Nonproducer cells that avoid the cost of production would outcompete producer cells and suppress cross-feeding (48). Direct benefits for the excretion of organic carbon by individual *Prochlorococcus* cells are therefore needed to explain cross-feeding interactions. Benefits of excreting organic carbon hypothesized for aerobic heterotrophs (26, 49–51) provide relevant clues, but do not fully translate to *Prochlorococcus* evolution (see *SI Appendix*, *SI Text* for further discussion).

**Integrating Evidence Across Levels of Organization Suggests a Unifying View of Evolution in *Prochlorococcus*.** To gain a better understanding of the evolution of *Prochlorococcus*, we mapped observations of its metabolism (Fig. 3 and *SI Appendix*, Fig. S1) onto its population structure (Fig. 1), growth and light physiology, and the macromolecular and elemental composition of cells. This suggests two evolutionary trends. First, in stable water columns, more recently diverged (HL) ecotypes experience a higher photosynthetic electron flux density [$\mu$mol electrons (g dry weight)$^{-1}$ time$^{-1}$], which can be parameterized as:

$$\nu_e = I\sigma_{PSII}\Phi_{PSII}, \quad [1]$$

where $I$ is light intensity ($\mu$mol photons m$^{-2}$ time$^{-1}$), $\sigma_{PSII}$ is the mass-normalized whole-cell photosystem II absorption cross-section [m$^2$ of PSII (g dry weight)$^{-1}$], and $\Phi_{PSII}$ is the quantum efficiency of PSII (electrons photon$^{-1}$). An increase in the cellular electron flux density along the *Prochlorococcus* phylogeny is suggested most obviously by the layering of the relative abundance of its ecotypes that emerges when the water column stratifies after a mixing event in the open ocean (Fig. 1), with the HL cells always dominating the surface waters (10–14). However, $\sigma_{PSII}$ also increases along the phylogeny, suggesting that more recently diverging strains also experience an increased electron flux at a given light level $I$. This increase in $\sigma_{PSII}$ is manifested in changes in the pigments (6, 9, 54, 55) and stoichiometry (56, 57) of the photosystems (Fig. 3 and *SI Appendix*, Fig. S1). These changes largely relinquish absorption of green and yellow light, but maintain or increase absorption of blue light—typifying the open ocean—in *Prochlorococcus* relative to *Synechococcus* (32, 58). At the same time *Prochlorococcus* is significantly smaller than *Synechococcus* (6), and cell mass decreases along its phylogeny (59), thus suggesting an increase in the mass-normalized absorption cross-section $\sigma_{PSII}$. Fewer comparative studies exist for the quantum efficiency of PSII ($\Phi_{PSII}$) but it appears to be roughly similar along the *Prochlorococcus* phylogeny (57). The increasing excretion of organic carbon by *Prochlorococcus* thus appears to reflect a more general trend that increases the total cellular throughput of electrons (Fig. 3). Various genes related to the protection and repair of light damage have been added in HL clades of *Prochlorococcus* (52, 53), suggesting that later divergences were primarily related to fortifying cellular machinery to allow cells to generate an increased electron flux at the highest photon fluxes near the surface (Fig. 3).

In addition to an increasing electron flux density ($\nu_e$), integrating evidence across levels suggests the evolution of *Prochlorococcus* also decreased its limiting nutrient flux density, $\nu_n$ [moles of $n$ (g dry weight)$^{-1}$ time$^{-1}$)]. For steady-state growth under constant conditions, $\nu_n$ can be parameterized as:

$$\nu_n = \mu Q_n, \quad [2]$$

where $\mu$ is the specific growth rate (time$^{-1}$) and $Q_n$ is the mass-normalized cellular quota of limiting nutrients [moles of $n$ (g dry weight)$^{-1}$]. A decreasing nutrient flux density during the evolution of *Prochlorococcus* is suggested by a decrease in its maximal intrinsic growth rate $\mu_{max}$ (time$^{-1}$) relative to *Synechococcus*

(6, 32) and an increased efficiency in its use of limiting nutrients. The latter is inferred from many features of *Prochlorococcus*, including less investment of N and P in the genome by reducing its size and guanine–cytosine content (60), decreased use of amino acids with N-rich side chains (61), a switch from P- to sulfolipid membranes (62, 63), and less Fe use in metabolism and photosynthetic machinery (33, 34) (*SI Appendix*, Fig. S1). These changes suggest a decreasing $Q_n$ for N, Fe, and P, the three main limiting nutrients in the oligotrophic oceans (64). An increasing $\nu_e$ coinciding with a decreasing $\nu_n$ over the course of *Prochlorococcus* evolution can be expressed as a single variable: the electron-to-nutrient flux ratio, $\nu_e/\nu_n$ (Fig. 3).

**Electron Flux and Nutrient Acquisition.** What are the selective pressures maximizing $\nu_e/\nu_n$ in *Prochlorococcus*? Photosynthetic electron flux transfers solar energy into metabolism via cofactors such ATP and NAD(P)H (65). An increased electron flux [$\mu$mol electrons (g dry weight)$^{-1}$ time$^{-1}$] thus suggests an increased metabolic rate [kJ of absorbed solar energy (g dry weight)$^{-1}$ time$^{-1}$]. This principle is exemplified by the increasing metabolic activity and ATP/ADP ratios of plant chloroplasts and cyanobacteria when they shift from darkness into light (66, 67). Furthermore, the highest $\nu_e/\nu_n$ phenotypes are the most recently diverging clades (Fig. 3), dominating near the surface where the solar energy supply is greatest and nutrient levels are lowest (Fig. 1), suggesting an advantage to higher metabolic rates at lower nutrient concentrations.

How metabolic rate affects nutrient uptake can be understood from Michaelis–Menten kinetics, which under strong nutrient limitation ($[n] \ll K_{M,n}$) simplifies to (68) (*SI Appendix*, *SI Text*):

$$\nu_n = [n]a_n^0 = V_{max}[n]/K_{M,n}, \qquad [3]$$

where $[n]$ is the nutrient concentration (moles of $n$ L$^{-1}$) and $a_n^0$ is the specific nutrient affinity [L (g dry weight)$^{-1}$ time$^{-1}$]. Specific affinity indicates how strongly cells absorb limiting nutrients (analogous to the pumping speed of a vacuum pump) and is equivalent to the saturated maximal nutrient uptake rate $V_{max}$ [moles of $n$ (g dry weight)$^{-1}$ time$^{-1}$] over the Michaelis constant $K_{M,n}$ (moles of $n$ L$^{-1}$) (68) (*SI Appendix*, Fig. S3). $V_{max}$ reflects the maximum handling rate for absorbed nutrients and is proportional to metabolic rate (68, 69). The free energy cost $\Delta_r G$ (kJ mol$^{-1}$) of nutrient transport scales with natural log of the ratio of internal to external nutrient concentrations (65) (*SI Appendix*, *SI Text*) and can become very large in the extremely nutrient-poor oligotrophic oceans (69). For example, the free energy cost of phosphate uptake in the oligotrophic oceans is far greater than the free energy gain of ATP hydrolysis unless the ATP/(ADP $\times$ P$_i$) ratio is increased drastically from commonly assumed metabolite concentrations of 1 mM for ATP, ADP, and P$_i$ (*SI Appendix*, *SI Text*). An analogous, but slightly different, situation occurs for ammonia ($NH_4^+$) uptake, which has the potential for a major futile cycle in the oligotrophic ocean, because its conjugate base $NH_3$ passively diffuses out of the cell (70) (*SI Appendix*, *SI Text*). It is therefore thought that cells poise their internal [$NH_4^+$] at the minimal viable value (71), which in turn similarly requires a significant increase in the ATP/(ADP $\times$ P$_i$) ratio to drive forward glutamine synthesis (glutamate + $NH_3$ + ATP $\rightleftharpoons$ glutamine + ADP + P$_i$), the central highway for nitrogen into metabolism (65). (See *SI Appendix*, *SI Text* for detailed calculations and discussion.) Finally, while kinetic bottleneck reactions can be driven forward by increasing the ATP/(ADP $\times$ P$_i$) ratio, this simultaneously increases the free energy cost of ATP synthesis, therefore requiring a greater proton motive force, and thus ultimately a greater photosynthetic electron flux (69).

The principles just outlined suggests that innovations increasing $\nu_e$ may lower the minimal subsistence concentration of limiting nutrients $[n]^*$ (the lowest value of $[n]$ at which net positive growth is possible). When growth and loss processes are relatively rapid and tightly coupled, microbial strains with the lowest $[n]^*$ dominate (72), suggesting that selection should favor such innovations. To understand how selection to lower $[n]^*$ shapes cells, we can substitute an expression for $V_{max}$ that assumes reversible kinetics (*SI Appendix*, *SI Text*) into Eq. **3**:

$$[n] = \frac{K_{M,n}}{V_{max}}\nu_n = \frac{K_{M,n}}{[E]k^+}\frac{\nu_n}{1 - e^{\Delta_r G/RT}}, \qquad [4]$$

where $[E]$ is the enzyme concentration [moles of enzyme (g dry weight)$^{-1}$]. $k^+$ is the rate constant [moles of $n$ (moles of enzyme)$^{-1}$ time$^{-1}$], $R$ is the gas constant (J K$^{-1}$ mol$^{-1}$), and $T$ is temperature (K). Eq. **4** suggests that there are two strategies for lowering $[n]^*$ (*SI Appendix*, Fig. S3). First, cells can modify the kinetics (decreasing $K_{M,n}$ and/or increasing $k^+, [E]$) and thermodynamics (decreasing $\Delta_r G$) of their metabolism, the latter by increasing $\nu_e$ as we have just argued. Second, cells can lower their $[n]^*$ by lowering their required flux of limiting nutrients $\nu_n$ (Eq. **4**), which can be achieved by lowering their minimal $Q_n$ [i.e., streamlining (73)] or their $\mu$ (Eq. **2**), both of which are apparent in the evolution of *Prochlorococcus* as discussed above. Optimizing kinetics/thermodynamics and decreasing $\nu_n$ can work synergistically, and both are helped by a decrease in cell mass, as is observed along the *Prochlorococcus* phylogeny (6, 59). That is, selection to lower $\nu_n$ allows a decrease in total cell mass by minimizing the mass dedicated to nonessential components (73). If the amount of metabolic enzyme and photosynthetic machinery is kept fixed, this decrease in total cell mass would increase both $[E]$ (68) and $\sigma_{PSII}$ (and thus $\nu_e$, which makes $\Delta_r G$ more negative). For nitrogen, increasing $\nu_e$ in turn provides an additional avenue for lowering $Q_N$ (and thus $\nu_N$), because pathways with a more negative $\Delta_r G$ require less protein biomass for a given flux (74). Thus, maximizing $\nu_e/\nu_n$ lowers the $[n]^*$ of cells by making the $\Delta_r G$ more negative (driving kinetic bottleneck reactions forward), thereby increasing the nutrient affinity (68, 69). As a result, the evolution of *Prochlorococcus* has driven nutrients to vanishingly low levels (<0.1 nM) in the oligotrophic oceans (64).

**Benefits of Excreting Organic Carbon.** If selection to lower $[n]^*$ drives the maximization of $\nu_e/\nu_n$, why should it lead to an increased excretion of organic carbon? We argue this ultimately emerges from mass and energy conservation. That is, in the presence of kinetic bottlenecks, cells can drive up their ATP/ADP ratio by increasing their ATP supply rate, but to maintain steady state, they must also increase ATP consumption rates (49, 69). [The same argument applies to the NAD(P)H/NAD(P) ratio.] This is consistent with observations that some nutrient-limited aerobic chemoheterotrophs have increased glucose uptake rates, increased levels of respiration, increased excretion of polysaccharides (whose synthesis from glucose requires ATP consumption), and a high flux through various ATP-consuming futile cycles (25, 26, 49). For photosynthetic cells $CO_2$-fixation is a major sink for ATP and NAD(P)H, but cells are limited in the carbon flux density, $\nu_C$, they can accommodate. This limit is proportional to growth rate (Eq. **2**), and, because selection to lower $[n]^*$ favors relatively slow-growing cells (Eq. **4**), it is lower in the oligotrophic oceans. Thus, we argue that excreted organic carbon represents a kind of "carbon exhaust" that allows cells to maximize their nutrient affinity by increasing their metabolic rate above limits arising from carbon saturation.

This general mechanism is further illustrated by expanding Eq. **4**. We assume that the electron flux must support carbon fixation sufficient to build biomass at a rate dictated by $\nu_n$, that biomass has an elemental stoichiometry $Q_n/Q_C$, that the efficiency of fixation is #C/#e (carbon atoms electron$^{-1}$), and that a fraction ($0<\beta<1$) of carbon is excreted/respired. #C/#e depends on the oxidation states of the carbon source, biomass, and excreted carbon. For example, if the carbon source is $CO_2$ and biomass and excreted carbon have the oxidation state $CH_2O$, then #C/#e is 1/4 (i.e., $CO_2 + 4e^- + 4H^+ \rightleftharpoons CH_2O +$

$H_2O$). Photoprotective mechanisms like the water–water cycle of PTOX (*SI Appendix*, Fig. S1) act to lower #C/#e. Together, these assumptions lead to the expression (see also *SI Appendix*, *SI Text*):

$$[n] = \frac{K_{M,n}}{[E]k^+}\frac{\nu_n}{1-e^{\Delta_r G/RT}} = \frac{K_{M,n}}{[E]k^+}\frac{Q_n}{Q_C}\frac{\nu_e(\#C/\#e)(1-\beta)}{1-e^{\Delta_r G/RT}}. \quad [5]$$

Thus, while increasing metabolic rate (i.e., lowering $\Delta_r G$) lowers $[n]^*$, it also acts to increase $[n]^*$ by increasing the carbon flux density, unless excess carbon is excreted [$\beta > 0$ and increasing faster than $\nu_e$(#C/#e)] (Eq. **5**). Selection to lower $[n]^*$ would thus favor a decrease in $\nu_n$ and simultaneous increases in $\nu_e$ and $\beta$ (carbon excretion), exactly as we observed for the evolution of *Prochlorococcus* (Fig. 3).

**Metabolic Rate, Ecosystem Biomass, and Coevolutionary Dynamics.** What are the evolutionary and ecological consequences of Eq. **5**? Focusing on the evolution of *Prochlorococcus*, it suggests that the layered population structure observed in stable water columns (Fig. 1) (10–14) reflects the sequential evolution of new ecotypes near the surface, each with increasing metabolic rates, drawing down limiting nutrients and restricting ancestral ecotypes to ever deeper waters (Fig. 4). This type of evolutionary dynamic in which a key innovation causes a population to expand along a shifted adaptive landscape produces adaptive radiations (75, 76) and has been argued to be the dominant contributor to global microbial diversity (77). This is consistent with observations that the broadly defined ecotypes of *Prochlorococcus* consist of hundreds of stable subpopulations that diverged millions of years ago (78). These are "niche constructing" adaptive radiations, since the shift in the adaptive landscape arises because new ecotypes chemically modify their own environment (Fig. 4) (79). Subpopulations form clusters defined by the acquisition of small cassettes of genes involved in electron transfer, redox stress, and/or synthesis of membrane polysaccharides (78). Increased production of the latter is a recognized outlet of excess reducing power (25, 26, 40). In addition to providing an electron sink, membrane polysaccharides also mediate biological interactions (e.g., with phage, grazers, or other bacteria), suggesting that an increase in electron flux could have produced ecological feedbacks that drove further differentiation within *Prochlorococcus* ecotypes (78) and in those with which it interacts (80). Lastly, this framework suggests that by promoting the fixation and excretion of increasing amounts of organic carbon as a by-product of increasing the nutrient affinity, the evolution of *Prochlorococcus* increased the long-term steady-state concentrations of dissolved organic carbon (DOC) in the oligotrophic oceans (Fig. 4), which are much higher (by a factor of up to ~2) than elsewhere in the ocean (81). Because several compounds that *Prochlorococcus* may be excreting are known iron-binding ligands, including polysaccharides (82) and carboxylic acids like citrate (83), it may, in turn, also play a key role in buffering trace metal bioavailability in these environments.

When extended to the ecosystem level, Eq. **5** provides a mechanistic view of how the evolution of all microbial cells in the open ocean is interconnected via the chemically coevolving environment (79, 84): Any innovation in any lineage that increases the energy flux and lowers nutrient concentrations (Fig. 4) pushes all other lineages to follow suit and adopt similar innovations. Unlike in the classic "Red Queen hypothesis," in which evolution is a zero-sum game (85), here, the evolutionary dynamic increases resource capture, and thereby biomass, of the ecosystem. [Similarly, a paleontological survey of the distribution and body size of marine animals also led to the conclusion that the energy flux and biomass of ecosystems increases over evolutionary time (86).] The imprint of this collective dynamic can be seen in the broadly convergent features of all oceanic microbes. Slow growth, small cell size, streamlined genomes and proteomes, and use of nonphospholipid membranes—signature features of *Prochlorococcus*—are observed across both autotrophic and heterotrophic microbes in the oligotrophic oceans (61, 73, 87–89). Some of the photosynthetic machinery modifications that increased the electron flux of *Prochlorococcus* (Fig. 3) are also seen in diatoms and picoeukaryotes (33, 90, 91). Many oceanic heterotrophs in turn supplement their energy supply from organics by capturing sunlight with proteorodhopsins (92) and possess electron drains in their respiratory electron transfer chains (93). In general, heterotrophic growth in the oligotrophic oceans favors metabolic rate over efficiency—the fraction of carbon taken up from the environment that is converted into biomass is one of the lowest of any aquatic environment on Earth (94). These observations are all consistent with the notion that the maximization of $\nu_e/\nu_n$, and thereby a lowering of steady-state nutrient concentrations (Eq. **5** and Fig. 4), has been a general evolutionary driving force in ocean ecosystems.

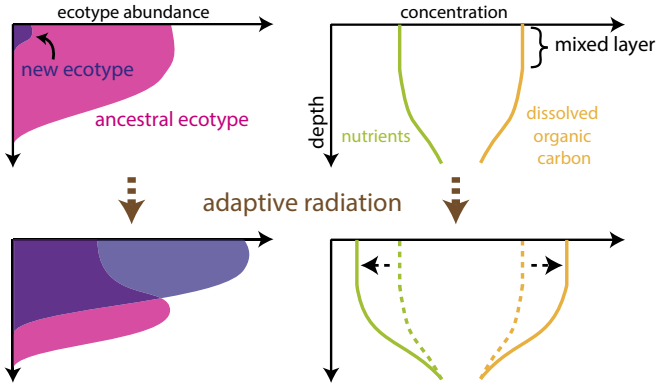


**Fig. 4.** The emergence of *Prochlorococcus* ecotypes. Eq. **5** suggests that innovations increasing $\nu_e/\nu_n$ trigger the emergence of new ecotypes (purple) that draw down limiting nutrients (*n*, green depth profile) in oceanic surface waters as they go through adaptive radiation. Nutrient drawdown near the surface increases ecosystem biomass and restricts ancestral ecotypes (pink) with a higher minimum subsistence nutrient concentration [*n*] to greater depths in the water column where nutrient levels remain higher. Finally, Eq. **5** suggests that by excreting increasing amounts of fixed carbon, while maximizing $\nu_e/\nu_n$, the evolution of *Prochlorococcus* has increased the long-term steady-state concentrations of DOC (orange depth profile).

**Emergence of Mutualism in Oceanic Microbial Ecosystems.** Finally, if lowering $[n]^*$ increases the excretion of organic carbon into the environment, it could produce new opportunities for cooccurring heterotrophs, like the ubiquitous and abundant SAR11 (73, 95). SAR11 requires pyruvate and either glycolate, glycine, serine, or glycine betaine (96); the latter four all feed into the same pathway that starts from glycolate (96). Furthermore, coastal SAR11 strains can replace pyruvate with glucose metabolized via glycolysis, whereas open ocean strains lack glycolysis and have an obligate requirement for pyruvate (97). Similar adaptations are not observed in freshwater strains of SAR11 (98). Thus, oceanic SAR11 populations have evolved a dependency on exactly the compounds (pyruvate and glycolate) that our metabolic reconstructions suggest emerged as excretion pathways in *Prochlorococcus* (Fig. 3 and *SI Appendix*, Fig. S1).

We mapped the distribution of metabolic genes across clades (*SI Appendix*, Table S2) onto the phylogeny of marine SAR11 clades to further reconstruct the evolution of their metabolic core (96–98) (Fig. 5 and *SI Appendix*, Fig. S4). We aimed to resolve the innovations of open ocean lineages and look for evidence of selection on pathway controls by looking for transporters in the vicinity of metabolic genes. As in *Prochlorococcus* (Fig. 3 and *SI Appendix*, Table S1), the metabolic core of SAR11 (*SI Appendix*, Fig. S4) evolved through a sequence of innovations (Fig. 5 and *SI Appendix*, Table S2), including the step-wise completion of the glyoxylate shunt and the well-documented switch

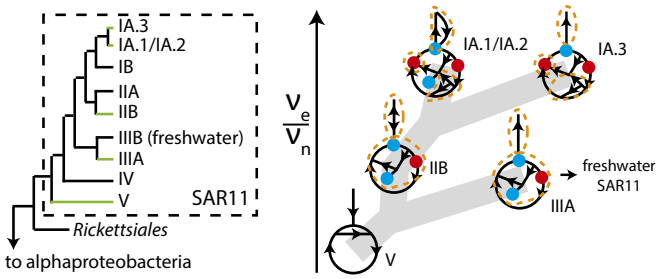


**Fig. 5.** Metabolic evolution of SAR11. Variants are shown in simplified form along a gradient of $\nu_e/\nu_n$. Dashed orange lines highlight innovations (*SI Appendix*, Fig. S4 and Table S2), which include disruptions or replacements of glycolysis (all branches), the step-wise completion of the glyoxylate shunt (from group V to IIB to all groups IA) and the gain and loss of excretion/uptake pathways. See main text for details. Excretion pathways are represented as red dots and uptake pathways as blue dots. This reconstruction is less certain than for *Prochlorococcus* because SAR11 has greater diversity (99, 100), and as highlighted in the phylogeny (included clades in green), many clades have no or few sequenced representatives (*SI Appendix*, Table S2). Several branches were therefore drawn as a polytomy.

from Emden–Meyerhoff–Parnass (EMP) to Entner–Doudoroff (ED) glycolysis (97). Glycolysis is disrupted in the 1.3A clade (97) (Fig. 5 and *SI Appendix*, Table S2), which is most abundant in surface waters where the *Prochlorococcus* HLII clade dominates (Fig. 1) (99, 100). Glycolate uptake is also lost in this SAR11 clade (Fig. 5 and *SI Appendix*, Table S2), which suggests that pyruvate produced by the *Prochlorococcus* HLII ecotype may have become its central source of carbon and energy (97). Finally, similar to *Prochlorococcus* (*SI Appendix*, Fig. S2), chromosome rearrangements positioned a series of transporter proteins near key metabolic genes in SAR11 (*SI Appendix*, Fig. S5), consistent with selection on the control of transport pathways. We identified putative import transporters for pyruvate and glycolate, and putative export transporters for citrate and malate, the latter exclusive to the 1A clade (Fig. 5 and *SI Appendix*, Fig. S5). The emergence of malate export in SAR11 would provide a potential source for the emergent malate uptake pathway of *Prochlorococcus* that is putatively activated at night (Fig. 3 and *SI Appendix*, Figs. S1 and S2).

Furthermore, the glyoxylate shunt is a TCA cycle bypass activated under redox stress in some microbes (101–103), while the evolutionary switch from EMP to the higher-rate ED variant of glycolysis has, in other microbes, been attributed to an increased energy supply (74). These observations are consistent with selection acting to maximize $\nu_e/\nu_n$ in both systems and thereby producing pathways that transfer pyruvate and glycolate from *Prochlorococcus* to SAR11 and malate from SAR11 to *Prochlorococcus*. Oligotrophic waters have nanomolar concentrations of pyruvate and glycolate, with midday maxima for the latter, consistent with biological cross-feeding synchronized with the input of sunlight, although abiotic photochemistry may also contribute (104, 105).

Additional evidence for metabolic mutualism in these systems comes from observations regarding hydrogen peroxide (HOOH), a by-product of biological electron transport, photochemistry, and other abiotic processes (106). *Prochlorococcus* and some later-diverging clades of SAR11 have lost HOOH-detoxifying catalase (*SI Appendix*, Tables S1 and S2), and *Prochlorococcus* grows better in the presence of bacteria retaining catalase (107, 108). This led to the "Black Queen" hypothesis, which argues that subpopulations of ecosystems can save essential nutrients by giving up inevitably shared functions (such as detoxifying the freely diffusible HOOH), so long as they are preserved by others in the ecosystem (109). Our reconstructions suggest that the loss of catalase in *Prochlorococcus* and SAR11 coincides with increased excretion of organic carbon, which provides carbon and energy for catalase-containing bacteria (109).

These observations suggest that metabolic mutualisms are self-amplifying feedback loops (110) that maximize the collective $\nu_e/\nu_n$, and thus total productivity, of ecosystems. Specifically, recycling otherwise wasted electrons through complementary excretion/uptake pathways increases the average $\nu_e$ of participating cells. Similarly, the loss of functions that are shared and require limiting nutrients (e.g., iron in catalase) in some members of the community decreases the average $\nu_n$. Mutualisms thus raise the $\nu_e/\nu_n$ of ecosystems—and lower the subsistence nutrient requirements of their cells (Eq. **5** and Fig. 4)—beyond what is possible for individual lineages in isolation. Because excreting organic carbon lowers the minimal subsistence nutrient requirements of individual cells, mutualisms of this kind are emergent properties of ecosystems and avoid public goods dilemmas (48). An upper bound may exist on the maximization of $\nu_e/\nu_n$ due to the minimal requirements of being an autonomous cell. As the smallest photosynthetic cell (6), *Prochlorococcus* may be closest to this limit, reinforcing the notion that it has a central role in shaping the features of ecosystems in the surface oceans.

**Are Plant Cells Microscopic Analogs of Oceanic Microbial Ecosystems?** It occurred to us that the metabolic organization of oceanic microbial ecosystems and green plant cells are similar (Fig. 6): Intermediates of lower glycolysis and photorespiration are central conduits of electron transfer from *Prochlorococcus* to SAR11 and from chloroplasts to mitochondria in plant cells, while TCA cycle intermediates facilitate electron transfer in the opposite direction in both systems (111–113). Similar patterns emerge at other levels of organization. Microbes other than *Prochlorococcus*/SAR11 in ocean communities, and organelles other than chloroplasts/mitochondria in plant cells, appear central to peroxide detoxification (108, 113). The heterotrophic bacteria SAR86 and SAR116 may be important for this function in the oligotrophic oceans, because they both possess catalase (114–116) and are abundant in warm stratified waters (117). *Prochlorococcus* and chloroplasts both have PTOX as an electron drain in their photosynthetic electron transfer chain, whereas SAR11 and mitochondria both have alternative oxidase (AOX) as an electron drain in their respiratory electron transfer chain (93, 113). Furthermore, like chloroplasts, *Prochlorococcus* uses chlorophyll *b* in addition to chlorophyll *a*, which has not been observed in cyanobacteria other than *Prochloron* and *Prochlorotrix* (6). Finally, organelles of plant cells have also undergone reductive genome evolution, and, for mitochondria, it has been argued that this increased the cellular power density of eukaryotes (118)—similar to what we argued for oceanic microbial ecosystems. The extensive convergence of plant cells and oceanic microbial ecosystems highlights the constraints that metabolism imposes on the large-scale structure of evolution (5) and suggests that the metabolic codependencies of eukaryotic organelles can evolve without the physical intimacy of endosymbiosis.

**Biospheric Self-Amplification and the Rise of Atmospheric Oxygen.** We have proposed that maximizing the metabolic rate of cells lowers their minimal subsistence nutrient requirements and that this is achieved by maximizing the cellular electron-to-nutrient flux ratio ($\nu_e/\nu_n$), while increasing the excretion of organic carbon (Eq. **5**). This leads to an evolutionary dynamic that increases total ecosystem biomass (Fig. 4) and paves the way for self-amplifying feedback loops that recycle organic carbon (Fig. 6) and reinforce the maximization of cellular metabolic rate at the ecosystem level. It has been argued that the hierarchical organization of pathways within metabolism reflects the outgrowth of self-amplifying feedbacks that increased the free energy consumption of the emerging biosphere (5, 119). Our framework extends those arguments into the world of phenotypically differentiated cells and microbial ecosystems, and is consistent with the theorem that the flow of energy through the biosphere promotes its self-organization into chemical cycles (2).

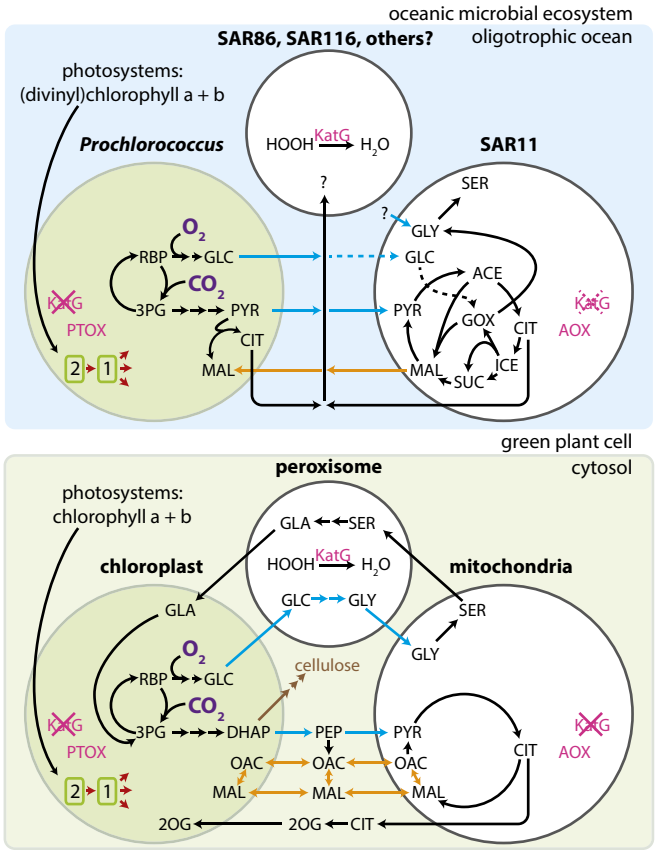


**Fig. 6.** The metabolic organization of *Prochlorococcus* and SAR11 and that of green plant cells. For simplicity, many reaction sequences are shown as single arrows without accurate stoichiometry. Blue/orange arrows indicate organic carbon flux through similar pathways between *Prochlorococcus* and SAR11 and between chloroplasts and mitochondria. The loss of glycolate uptake in the open ocean 1A.3 clade (Fig. 5) is indicated by a dashed arrow. The loss of catalase in *Prochlorococcus* is indicated by a crossed-out KatG gene, while this cross-out is dashed for SAR11 to indicate the loss of catalase in some of its later branching clades. In plant cells, catalase is similarly located in the peroxisome and not chloroplasts/mitochondria (111–113) as indicated by the crossed-out KatG genes. PTOX and AOX provide electron drains in the electron transport chains of both systems, and chloroplasts and *Prochlorococcus* both use chlorophyll *b* as well as *a* (6). 2OG, 2-oxoglutarate; 3PG, 3-phosphoglycerate; ACE, acetyl-CoA; KatG, catalase; CIT, citrate; DHAP, dihydroxyacetone phosphate; GLA, glycerate; GLC, glycolate; GLY, glycine; GOX, glyoxylate, ICE, isocitrate; MAL, malate; OAC, oxaloacetate; PEP, phosphoenoylpyruvate; PYR, pyruvate; RBP, ribulose bisphosphate; SER, serine; SUC, succinate.

Our framework has implications for Earth history. If biospheric self-amplification driven by the sun enhanced the burial of organics and carbonates (120, 121) simply by increasing their production, it would help explain the drawdown of atmospheric $CO_2$ and the rise of atmospheric $O_2$ across several stages of Earth history (122, 123). Perhaps not coincidentally, marine picocyanobacteria are estimated to have emerged near the transition from the Neoproterozoic (1,000–541 Ma) to the Phanerozoic (541 Ma to present) (124, 125), when sediments indicate the occurrence of global glaciations (126, 127), global carbon cycle perturbations (128–130), enhanced organic carbon burial (120, 121), and a second major rise in atmospheric $O_2$ toward modern levels (123, 131–133).

The proposed evolutionary dynamic (Fig. 4) may provide insights into the Neoproterozoic–Phanerozoic rise in atmospheric oxygen. It has been argued that after the Great Oxidation Event (GOE) the deep Proterozoic oceans remained largely anoxic and euxinic (rich in $H_2S$) (134). Recent studies support anoxia, but suggest that the Proterozoic oceans were instead largely ferruginous (rich in $Fe^{2+}$), with euxinia restricted to productive continental margins (135–137). It was argued this general redox structure persisted because of N/Mo limitation (138, 139), with Mo scavenged by $H_2S$ even with only limited global euxinia (137), and P limitation due to its scavenging by abundant $Fe^{2+}$ (140). We suggest an additional negative feedback involving iron, the most widely used metal cofactor for biological electron transfer (141). The free $O_2$ produced during the rise of oxygenic photosynthesis transformed iron from its soluble $Fe^{2+}$ form into its insoluble $Fe^{3+}$ form (142), effectively causing early oxygenic photosynthesizers to self-limit their expansion in the global oceans by locally extinguishing available iron. Extant oceanic microbes surmount this negative feedback on photosynthetic electron transfer through reduced cellular Fe demands (33, 90, 91) (*SI Appendix*, Fig. S1), and through Fe- ligation by DOC (143), including polysaccharides (82), citrate (83), and other carboxylic acids, all of which may be excreted by marine picocyanobacteria (37, 39) (*SI Appendix*, Fig. S1). Polysaccharides and small carboxylic acids also enhance the dissolution of minerals (144), and minerals in wind-blown dust are a major source of Fe (145) and P (146) to the surface oceans. Thus, we hypothesize that the evolution of marine picocyanobacteria (Fig. 4) increased both the bioavailability and the overall supply of iron under aerobic conditions and helped transform the oceans from an anoxic state rich in free iron (135, 136) to an oxygenated state (131, 133) with DOC-bound iron. This positive iron–DOC feedback, strengthened by an increased metabolic rate, was critical in pushing the marine biosphere past a major evolutionary bottleneck and paved the way for an expansion of oceanic oxygenic photosynthesis and a rise in atmospheric $O_2$ (123).

Sedimentary and genomic records suggest several additional positive feedbacks that could have pushed forth the Phanerozoic oxygenation of the ocean. Increased Fe bioavailability under aerobic conditions coinciding with the drawdown of nitrogen (Fig. 4) would have created opportunities for $N_2$-fixers, while ocean oxygenation would have lifted their Mo-limitation by suppressing euxinia (137, 138), together increasing the supply of nitrogen to the oceans (124, 138, 139). This is consistent with the suggested overlap in the rise of marine picocyanobacteria and planktonic $N_2$-fixers (124, 125). Furthermore, sediments suggest an increase in oceanic P levels after the Neoproterozoic, and it was argued that this was because a drop in $Fe^{2+}$ concentrations lessened the scavenging of P (140). We add that if enhanced DOC-dissolution of minerals from dust enhanced the oceanic iron supply under aerobic conditions, as we argued above, it could have also enhanced the P supply (146), thus contributing to the reconstructed rise in P levels (140).

These scenarios are similar to those of how the rise of land plants impacted the Earth system. Nutrient-limited plants leach Fe, P, and other nutrients from rocks by excreting small carboxylic acids from their roots (which suggests an increased metabolic rate—Eq. **5**) (147). It has therefore been argued that plant colonization of the continents during the Phanerozoic increased the weathering of rocks, and, in turn, the precipitation of carbonates, which, together with the increased burial of plant-derived organics, resulted in a drawdown of atmospheric $CO_2$ and a rise in atmospheric $O_2$ (148–150).

The convergent metabolic evolution of oceanic microbial ecosystems and land plants (Fig. 6), which, we have argued, may have impacted the Earth system in similar ways, suggests the temporal profile of the Earth's oxygenation (122, 123) may be constrained by two biological stages. The first consisted of the expansion of self-damping cyanobacterial $O_2$-photosynthesis in shallow aquatic environments and is associated with the GOE (122, 123). The second consisted of the global expansion of eukaryotic or "eukaryote-like" $O_2$-photosynthesis—both onto the continents and into the deep open ocean (Fig. 6)—with a higher metabolic rate and correspondingly greater ability to mobilize Fe and P under oxidizing conditions, and is associated

with the Neoproterozoic Oxidation Event (122, 123, 132, 142). Genomic studies estimate that chloroplast endosymbiosis leading to the rise of all photosynthetic eukaryotes occurred between the late Paleoproterozoic (2,500–1,600 Ma) and the early Neoproterozoic (151–154). Paleontological studies in turn find a significantly increased fossil diversity of eukaryotes (including photosynthetic eukaryotes) in the Neoproterozoic (155, 156), whose increasing body sizes and fecal pellets could have moreover strengthened the export and burial of organic carbon from the oceans (157, 158).

As a final note, one could argue that the emergence of modern human societies is a variant of the general framework we propose. As our populations expanded and extracted ever more electrons from fossil fuels, we have increased global $CO_2$, while drawing down natural resources and global $O_2$ (albeit a small amount relative to the contemporary inventory for the latter) (159, 160). In the process, we have become increasingly socially, technologically, and economically interconnected, analogous to what we have observed in the evolution of oceanic microbial ecosystems and plant cells. As in those systems, this has increased our collective ability to harvest more difficult-to-access natural resources. Managing the biogeochemical perturbation that our global emergence is imposing on the Earth system is one of humanity's greatest challenges.

## Materials and Methods

We analyzed 56 genomes of cyanobacteria representative of the diversity of this clade (161) obtained from the UniProt website, 56 genomes of *Prochlorococcus* and marine *Synechococcus* (162), and 16 SAR11 genomes obtained from the National Center for Biotechnology Information website. We searched these genomes for the presence and absence of a set of reference enzymes (*SI Appendix*, Tables S1 and S2) using the BLASTp and tBLASTn algorithms (163). We reconstructed phylometabolic trees (Fig. 2) by mapping the distributions of metabolic genes onto the phylogenies of *Prochlorococcus* (Figs. 1 and 3) and SAR11 (Fig. 5).

**ACKNOWLEDGMENTS.** We thank the reviewers for critical and insightful reviews, and we thank Jamie Becker, Shane Hogle, and John Casey for comments on an earlier version of our manuscript. R.B. is a Simons Foundation Fellow of the Life Sciences Research Foundation. This work was supported by Simons Foundation Grant SCOPE 329108 (to S.W.C. and M.J.F.); Gordon and Betty Moore Foundation Grants 3778 (to M.J.F.) and 495.01 (to S.W.C.); and by the NSF Center for Microbial Oceanography Research and Education (S.W.C.). R.B. dedicates this work to the memory of Harold Morowitz, a pioneer in the study of biological energy flow, whose theories and approach to studying life were central in shaping the core ideas of this work.

1. Schrödinger E (1944) What Is Life? The Physical Aspect of the Living Cell (Cambridge Univ Press, Cambridge, UK).
2. Morowitz HJ (1968) Energy Flow in Biology; Biological Organization as a Problem in Thermal Physics (Academic, New York).
3. Brown JH, Gillooly JF, Allen AP, Savage VM, West GB (2004) Toward a metabolic theory of ecology. *Ecology* 85(7):1771–1789.
4. Falkowski PG, Fenchel T, Delong EF (2008) The microbial engines that drive earth's biogeochemical cycles. *Science* 320(5879):1034–1039.
5. Braakman R, Smith E (2013) The compositional and evolutionary logic of metabolism. *Phys Biol* 10(1):011001.
6. Chisholm SW, et al. (1988) A novel free-living prochlorophyte abundant in the oceanic euphotic zone. *Nature* 334:340–343.
7. Partensky F, Hess W, Vaulot D (1999) *Prochlorococcus,* a marine photosynthetic prokaryote of global significance. *Microbiol Mol Biol Rev* 63(1):106–127.
8. Flombaum P, et al. (2013) Present and future global distributions of the marine cyanobacteria *Prochlorococcus* and *Synechococcus*. *Proc Natl Acad Sci USA* 110(24):9824–9829.
9. Scanlan DJ, et al. (2009) Ecological genomics of marine picocyanobacteria. *Microbiol Mol Biol Rev* 73(2):249–299.
10. Johnson ZI, et al. (2006) Niche partitioning among *Prochlorococcus* ecotypes along ocean-scale environmental gradients. *Science* 311(5768):1737–1740.
11. Bouman HA, et al. (2006) Oceanographic basis of the global surface distribution of *Prochlorococcus* ecotypes. *Science* 312(5775):918–921.
12. Malmstrom RR, et al. (2010) Temporal dynamics of *Prochlorococcus* ecotypes in the atlantic and pacific oceans. *ISME J* 4(10):1252–1264.
13. Moore LR, Rocap G, Chisholm SW (1998) Physiology and molecular phylogeny of coexisting *Prochlorococcus* ecotypes. *Nature* 393(6684):464–467.
14. West NJ, Scanlan DJ (1999) Niche-partitioning of *Prochlorococcus* populations in a stratified water column in the eastern north atlantic ocean. *Appl Env Microbiol* 65(6):2585–2591.
15. Braakman R, Smith E (2012) The emergence and early evolution of biological carbon-fixation. *PLoS Comput Biol* 8(4):e1002455.
16. Braakman R, Smith E (2014) Metabolic evolution of a deep-branching hyperthermophilic chemoautotrophic bacterium. *PLoS One* 9(2):e87950.
17. Badger MR, Hanson D, Price GD (2002) Evolution and diversity of $CO_2$ concentrating mechanisms in cyanobacteria. *Funct Plant Biol* 29(3):161–173.
18. Tabita FR, et al. (2007) Function, structure, and evolution of the rubisco-like proteins and their rubisco homologs. *Microbiol Mol Biol Rev* 71(4):576–599.
19. Abdul-Rahman F, Petit E, Blanchard JL (2013) The distribution of polyhedral bacterial microcompartments suggests frequent horizontal transfer and operon reassembly. *J Phylogenetics Evol Biol* 1(4):118.
20. Zhang S, Bryant DA (2011) The tricarboxylic acid cycle in cyanobacteria. *Science* 334(6062):1551–1553.
21. Chen X, et al. (2016) The Entner–Doudoroff pathway is an overlooked glycolytic route in cyanobacteria and plants. *Proc Natl Acad Sci USA* 113(19):5441–5446.
22. Dufresne A, et al. (2003) Genome sequence of the cyanobacterium *Prochlorococcus marinus* SS120, a nearly minimal oxyphototrophic genome. *Proc Natl Acad Sci USA* 100(17):10020–10025.
23. Eisenhut M, et al. (2008) The photorespiratory glycolate metabolism is essential for cyanobacteria and might have been conveyed endosymbiontically to plants. *Proc Natl Acad Sci USA* 105(44):17199–17204.
24. Fogg GE (1983) The ecological significance of extracellular products of phytoplankton photosynthesis. *Bot Mar* 26(1):3–14.
25. Neijssel O, Tempest D (1975) The regulation of carbohydrate metabolism in *Klebsiella aerogenes* NCTC 418 organisms, growing in chemostat culture. *Arch Microbiol* 106(3):251–258.
26. Russell JB, Cook GM (1995) Energetics of bacterial growth: Balance of anabolic and catabolic reactions. *Microbiol Rev* 59(1):48–62.
27. Dauner M, Storni T, Sauer U (2001) *Bacillus subtilis* metabolism and energetics in carbon-limited and excess-carbon chemostat culture. *J Bacteriol* 183(24):7308–7317.
28. Vemuri G, Eiteman M, McEwen J, Olsson L, Nielsen J (2007) Increasing NADH oxidation reduces overflow metabolism in *Saccharomyces cerevisiae*. *Proc Natl Acad Sci USA* 104(7):2402–2407.
29. McKinlay JB, Harwood CS (2010) Carbon dioxide fixation as a central redox cofactor recycling mechanism in bacteria. *Proc Natl Acad Sci USA* 107(26):11669–11675.
30. Hopkinson BM, Young JN, Tansik AL, Binder BJ (2014) The minimal $CO_2$-concentrating mechanism of *Prochlorococcus* spp. MED4 is effective and efficient. *Plant Physiol* 166(4):2205–2217.
31. Hartmann M, et al. (2014) Efficient $CO_2$ fixation by surface *Prochlorococcus* in the Atlantic Ocean. *ISME J* 8(11):2280–2289.
32. Moore LR, Goericke R, Chisholm SW (1995) Comparative physiology of *Synechococcus* and *Prochlorococcus*: Influence of light and temperature on growth, pigments, fluorescence and absorptive properties. *Mar Ecol Prog Ser* 116(1):259–275.
33. Bailey S, et al. (2008) Alternative photosynthetic electron flow to oxygen in marine *Synechococcus*. *Biochim Biophys Acta* 1777(3):269–276.
34. Mackey KR, Paytan A, Grossman AR, Bailey S (2008) A photosynthetic strategy for coping in a high-light, low-nutrient environment. *Limnol Oceanogr* 53(3):900–913.
35. Mella-Flores D, et al. (2012) *Prochlorococcus* and *Synechococcus* have evolved different adaptive mechanisms to cope with light and uv stress. *Front Microbiol* 3:285.
36. Bagby SC, Chisholm SW (2015) Response of *Prochlorococcus* to varying $CO_2$: $O_2$ ratios. *ISME J* 9(10):2232–2245.
37. Bertlisson S, Berglund O, Pullin MJ, Chisholm SW (2005) Release of dissolved organic matter by *Prochlorococcus*. *Vie et Milieu* 55(3-4):225–232.
38. Bateson MM, Ward DM (1988) Photoexcretion and fate of glycolate in a hot spring cyanobacterial mat. *Appl Environ Microbiol* 54(7):1738–1743.
39. Biddanda B, Benner R (1997) Carbon, nitrogen, and carbohydrate fluxes during the production of particulate and dissolved organic matter by marine phytoplankton. *Limnol Oceanogr* 42(3):506–518.
40. Myklestad SM (1995) Release of extracellular products by phytoplankton with special emphasis on polysaccharides. *Sci Total Environ* 165(1):155–164.
41. Li YF, Costello JC, Holloway AK, Hahn MW (2008) 'Reverse ecology' and the power of population genomics. *Evolution* 62(12):2984–2994.
42. Zinser ER, et al. (2009) Choreography of the transcriptome, photophysiology, and cell cycle of a minimal photoautotroph, *Prochlorococcus*. *PLoS One* 4(4):e5135.
43. Waldbauer JR, Rodrigue S, Coleman ML, Chisholm SW (2012) Transcriptome and proteome dynamics of a light-dark synchronized bacterial cell cycle. *PLoS One* 7(8):e43432.
44. Bailey S, Mann NH, Robinson C, Scanlan DJ (2005) The occurrence of rapidly reversible non-photochemical quenching of chlorophyll a fluorescence in cyanobacteria. *FEBS Lett* 579(1):275–280.
45. Kulk G, van de Poll WH, Visser RJ, Buma AG (2011) Distinct differences in photoacclimation potential between prokaryotic and eukaryotic oceanic phytoplankton. *J Exp Mar Biol Ecol* 398(1):63–72.
46. Falkowski PG, LaRoche J (1991) Acclimation to spectral irradiance in algae. *J Phycol* 27(1):8–14.
47. Walters RG (2005) Towards an understanding of photosynthetic acclimation. *J Exp Bot* 56(411):435–447.
48. West SA, Griffin AS, Gardner A, Diggle SP (2006) Social evolution theory for microorganisms. *Nat Rev Microbiol* 4(8):597–607.
49. Neijssel O, Tempest D (1976) The role of energy-spilling reactions in the growth of *Klebsiella aerogenes* NCTC 418 in aerobic chemostat culture. *Arch Microbiol* 110(2-3):305–311.

50. Molenaar D, van Berlo R, de Ridder D, Teusink B (2009) Shifts in growth strategies reflect tradeoffs in cellular economics. *Mol Syst Biol* 5(1):323.
51. Basan M, et al. (2015) Overflow metabolism in *Escherichia coli* results from efficient proteome allocation. *Nature* 528(7580):99–104.
52. Kettler GC, et al. (2007) Patterns and implications of gene gain and loss in the evolution of *Prochlorococcus*. *PLoS Genet* 3(12):e231.
53. Partensky F, Garczarek L (2010) *Prochlorococcus*: Advantages and limits of minimalism. *Annu Rev Mar Sci* 2:305–331.
54. Goericke R, Repeta DJ (1992) The pigments of *Prochlorococcus marinus*: The presence of divinylchlorophyll a and b in a marine procaryote. *Limnol Oceanogr* 37(2):425–433.
55. Bibby T, Nield J, Partensky F, Barber J (2001) Oxyphotobacteria: Antenna ring around photosystem I. *Nature* 413(6856):590–590.
56. Bibby T, Mary I, Nield J, Partensky F, Barber J (2003) Low-light-adapted *Prochlorococcus* species possess specific antennae for each photosystem. *Nature* 424(6952):1051–1054.
57. Zorz JK, et al. (2015) The RUBISCO to photosystem II ratio limits the maximum photosynthetic rate in picocyanobacteria. *Life (Basel)* 5(1):403–417.
58. Morel A, Ahn YH, Partensky F, Vaulot D, Claustre H (1993) *Prochlorococcus* and *Synechococcus*: A comparative study of their optical properties in relation to their size and pigmentation. *J Mar Res* 51(3):617–649.
59. Cermak N, et al. (2017) Direct single-cell biomass estimates for marine bacteria via Archimedes' principle. *ISME J* 11(3):825–828.
60. Dufresne A, Garczarek L, Partensky F (2005) Accelerated evolution associated with genome reduction in a free-living prokaryote. *Genome Biol* 6(2):R14.
61. Grzymski JJ, Dussaq AM (2012) The significance of nitrogen cost minimization in proteomes of marine microorganisms. *ISME J* 6(1):71–80.
62. Van Mooy BA, Rocap G, Fredricks HF, Evans CT, Devol AH (2006) Sulfolipids dramatically decrease phosphorus demand by picocyanobacteria in oligotrophic marine environments. *Proc Natl Acad Sci USA* 103(23):8607–8612.
63. Van Mooy BA, et al. (2009) Phytoplankton in the ocean use non-phosphorus lipids in response to phosphorus scarcity. *Nature* 458(7234):69–72.
64. Moore C, et al. (2013) Processes and patterns of oceanic nutrient limitation. *Nat Geosci* 6(9):701–710.
65. Lengeler JW, Drews G, Schlegel HG, eds (1999) *Biology of the Prokaryotes* (Thieme, Stuttgart, Germany).
66. Gardeström P, Wigge B (1988) Influence of photorespiration on ATP/ADP ratios in the chloroplasts, mitochondria, and cytosol, studied by rapid fractionation of barley (*Hordeum vulgare*) protoplasts. *Plant Physiol* 88(1):69–76.
67. Rust MJ, Golden SS, O'Shea EK (2011) Light-driven changes in energy metabolism directly entrain the cyanobacterial circadian oscillator. *Science* 331(6014):220–223.
68. Button D (1991) Biochemical basis for whole-cell uptake kinetics: Specific affinity, oligotrophic capacity, and the meaning of the Michaelis constant. *Appl Environ Microbiol* 57(7):2033–2038.
69. Harder W, Dijkhuizen L (1983) Physiological responses to nutrient limitation. *Ann Rev Microbiol* 37(1):1–23.
70. Kleiner D (1985) Bacterial ammonium transport. *FEMS Microbiol Lett* 32(2):87–100.
71. Boogerd FC, et al. (2011) AmtB-mediated $NH_3$ transport in prokaryotes must be active and as a consequence regulation of transport by GlnK is mandatory to limit futile cycling of $NH_4^+/NH_3$. *FEBS Lett* 585(1):23–28.
72. Tilman D (1977) Resource competition between plankton algae: An experimental and theoretical approach. *Ecology* 58(2):338–348.
73. Giovannoni SJ, et al. (2005) Genome streamlining in a cosmopolitan oceanic bacterium. *Science* 309(5738):1242–1245.
74. Flamholz A, Noor E, Bar-Even A, Liebermeister W, Milo R (2013) Glycolytic strategy as a tradeoff between energy yield and protein cost. *Proc Natl Acad Sci USA* 110(24):10039–10044.
75. Simpson GG (1944) Tempo and Mode in Evolution (Columbia Univ Press, New York).
76. Simpson GG (1955) Major Features of Evolution (Columbia Univ Press, New York).
77. O'Dwyer JP, Kembel SW, Sharpton TJ (2015) Backbones of evolutionary history test biodiversity theory for microbes. *Proc Natl Acad Sci USA* 112(27):8356–8361.
78. Kashtan N, et al. (2014) Single-cell genomics reveals hundreds of coexisting subpopulations in wild. *Science* 344(6182):416–420.
79. Odling-Smee FJ, Laland KN, Feldman MW (2003) Niche Construction: The Neglected Process in Evolution (Princeton Univ Press, Princeton), No. 37.
80. Erwin DH (2005) Seeds of diversity. *Science* 308(5729):1752–1753.
81. Hansell DA, Carlson CA, Repeta DJ, Schlitzer R (2009) Dissolved organic matter in the ocean: A controversy stimulates new insights. *Oceanography* 22(4):202–211.
82. Hassler CS, Schoemann V, Nichols CM, Butler EC, Boyd PW (2011) Saccharides enhance iron bioavailability to southern ocean phytoplankton. *Proc Natl Acad Sci USA* 108(3):1076–1081.
83. Roe KL, Barbeau KA (2014) Uptake mechanisms for inorganic iron and ferric citrate in *Trichodesmium erythraeum* IMS101. *Metallomics* 6(11):2042–2051.
84. Jones CG, Lawton JH, Shachak M (1994) Organisms as ecosystem engineers. *Oikos* 69(3):373–386.
85. Van Valen L (1973) A new evolutionary law. *Evol Theory* 1:1–30.
86. Bambach RK (1993) Seafood through time: Changes in biomass, energetics, and productivity in the marine ecosystem. *Paleobiology* 19(03):372–397.
87. Sunda WG, Huntsman SA (1997) Interrelated influence of iron, light and cell size on marine phytoplankton growth. *Nature* 390(6658):389–392.
88. Swan BK, et al. (2013) Prevalent genome streamlining and latitudinal divergence of planktonic bacteria in the surface ocean. *Proc Natl Acad Sci USA* 110(28):11463–11468.
89. Sebastián M, et al. (2016) Lipid remodelling is a widespread strategy in marine heterotrophic bacteria upon phosphorus deficiency. *ISME J* 10(4):968–978.
90. Strzepek RF, Harrison PJ (2004) Photosynthetic architecture differs in coastal and oceanic diatoms. *Nature* 431(7009):689–692.
91. Cardol P, et al. (2008) An original adaptation of photosynthesis in the marine green alga ostreococcus. *Proc Natl Acad Sci USA* 105(22):7881–7886.
92. Béja O, et al. (2000) Bacterial rhodopsin: Evidence for a new type of phototrophy in the sea. *Science* 289(5486):1902–1906.
93. McDonald AE, Vanlerberghe GC (2005) Alternative oxidase and plastoquinol terminal oxidase in marine prokaryotes of the Sargasso Sea. *Gene* 349:15–24.
94. Del Giorgio PA, Cole JJ (1998) Bacterial growth efficiency in natural aquatic systems. *Annu Rev Ecol Syst* 29:503–541.
95. Morris RM, et al. (2002) SAR11 clade dominates ocean surface bacterioplankton communities. *Nature* 420(6917):806–810.
96. Carini P, Steindler L, Beszteri S, Giovannoni SJ (2013) Nutrient requirements for growth of the extreme oligotroph '*Candidatus* Pelagibacter ubique' HTCC1062 on a defined medium. *ISME J* 7(3):592–602.
97. Schwalbach M, Tripp H, Steindler L, Smith D, Giovannoni S (2010) The presence of the glycolysis operon in SAR11 genomes is positively correlated with ocean productivity. *Environ Microbiol* 12(2):490–500.
98. Eiler A, et al. (2016) Tuning fresh: Radiation through rewiring of central metabolism in streamlined bacteria. *ISME J* 10(8):1902–1914.
99. Brown MV, et al. (2012) Global biogeography of SAR11 marine bacteria. *Mol Syst Biol* 8(1):595.
100. Vergin KL, et al. (2013) High-resolution SAR11 ecotype dynamics at the Bermuda Atlantic Time-series Study site by phylogenetic placement of pyrosequences. *ISME J* 7(7):1322–1332.
101. Fischer E, Sauer U (2003) A novel metabolic cycle catalyzes glucose oxidation and anaplerosis in hungry *Escherichia coli*. *J Biol Chem* 278(47):46446–46451.
102. Liu Y, et al. (2003) Transcriptome dynamics of *Deinococcus radiodurans* recovering from ionizing radiation. *Proc Natl Acad Sci USA* 100(7):4191–4196.
103. Beste DJ, et al. (2011) 13c metabolic flux analysis identifies an unusual route for pyruvate dissimilation in mycobacteria which requires isocitrate lyase and carbon dioxide fixation. *PLoS Pathog* 7(7):e1002091.
104. Kieber DJ, Mopper K (1987) Photochemical formation of glyoxylic and pyruvic acids in seawater. *Marine Chem* 21(2):135–149.
105. Leboulanger C, Oriol L, Jupin H, Desolas-gros C (1997) Diel variability of glycolate in the eastern tropical Atlantic Ocean. *Deep Sea Res Oceanogr Res Paper* 44(12):2131–2139.
106. Yuan J, Shiller AM (2005) Distribution of hydrogen peroxide in the northwest Pacific Ocean. *Geochem Geophys Geosyst* 6(9):Q09M02.
107. Morris JJ, Kirkegaard R, Szul MJ, Johnson ZI, Zinser ER (2008) Facilitation of robust growth of *Prochlorococcus* colonies and dilute liquid cultures by 'helper' heterotrophic bacteria. *Appl Environ Microbiol* 74(14):4530–4534.
108. Morris JJ, Johnson ZI, Szul MJ, Keller M, Zinser ER (2011) Dependence of the cyanobacterium *Prochlorococcus* on hydrogen peroxide scavenging microbes for growth at the ocean's surface. *PLoS One* 6(2):e16805.
109. Morris JJ, Lenski RE, Zinser ER (2012) The black queen hypothesis: Evolution of dependencies through adaptive gene loss. *MBio* 3(2):e00036–e00012.
110. Eigen M, Schuster P (1977) The hypercycle. A principle of natural self-organization. *Naturwissenschaften* 64(11):541–565.
111. Hoefnagel MH, Atkin OK, Wiskich JT (1998) Interdependence between chloroplasts and mitochondria in the light and the dark. *Biochim Biophys Acta* 1366(3):235–255.
112. Raghavendra AS, Padmasree K (2003) Beneficial interactions of mitochondrial metabolism with photosynthetic carbon assimilation. *Trends Plant Sci* 8(11):546–553.
113. Noctor G, De Paepe R, Foyer CH (2007) Mitochondrial redox biology and homeostasis in plants. *Trends Plant Sci* 12(3):125–134.
114. Oh HM, et al. (2010) Complete genome sequence of '*Candidatus Puniceispirillum marinum*' IMCC1322, a representative of the SAR116 clade in the Alphaproteobacteria. *J Bacteriol* 192(12):3240–3241.
115. Grote J, et al. (2011) Draft genome sequence of strain HIMB100, a cultured representative of the SAR116 clade of marine alphaproteobacteria. *Stand Genomic Sci* 5(3):269–278.
116. Dupont CL, et al. (2012) Genomic insights to sar86, an abundant and uncultivated marine bacterial lineage. *ISME J* 6(6):1186–1199.
117. Treusch AH, et al. (2009) Seasonality and vertical structure of microbial communities in an ocean gyre. *ISME J* 3(10):1148–1163.
118. Lane N, Martin W (2010) The energetics of genome complexity. *Nature* 467(7318):929–934.
119. Smith E, Morowitz HJ (2004) Universality in intermediary metabolism. *Proc Natl Acad Sci USA* 101(36):13168–13173.
120. Des Marais DJ, Strauss H, Summons RE, Hayes J (1992) Carbon isotope evidence for the stepwise oxidation of the proterozoic environment. *Nature* 359:605–609.
121. Krissansen-Totton J, Buick R, Catling DC (2015) A statistical analysis of the carbon isotope record from the archean to phanerozoic and implications for the rise of oxygen. *Am J Sci* 315(4):275–316.
122. Holland HD (2006) The oxygenation of the atmosphere and oceans. *Philos Trans R Soc Lond B Biol Sci* 361(1470):903–915.
123. Lyons TW, Reinhard CT, Planavsky NJ (2014) The rise of oxygen in earth's early ocean and atmosphere. *Nature* 506(7488):307–315.
124. Sánchez-Baracaldo P, Ridgwell A, Raven JA (2014) A neoproterozoic transition in the marine nitrogen cycle. *Curr Biol* 24(6):652–657.
125. Sánchez-Baracaldo P (2015) Origin of marine planktonic cyanobacteria. *Sci Rep* 5:17418.

126. Kirschvink JL (1992) Late proterozoic low-latitude global glaciation: The snowball earth. *The Proterozoic Biosphere: A Multidisciplinary Study*, eds Schopf JW, Klein C, Des Marais D (Cambridge Univ Press, Cambridge, UK), pp 51–52.
127. Hoffman PF, Kaufman AJ, Halverson GP, Schrag DP (1998) A neoproterozoic snowball earth. *Science* 281(5381):1342–1346.
128. Knoll A, Hayes J, Kaufman A, Swett K, Lambert I (1986) Secular variation in carbon isotope ratios from upper proterozoic successions of Svalbard and East Greenland. *Nature* 321(6073):832–838.
129. Rothman DH, Hayes JM, Summons RE (2003) Dynamics of the neoproterozoic carbon cycle. *Proc Natl Acad Sci USA* 100(14):8124–8129.
130. Grotzinger JP, Fike DA, Fischer WW (2011) Enigmatic origin of the largest-known carbon isotope excursion in earth's history. *Nat Geosci* 4(5):285–292.
131. Fike D, Grotzinger J, Pratt L, Summons R (2006) Oxidation of the ediacaran ocean. *Nature* 444(7120):744–747.
132. Och LM, Shields-Zhou GA (2012) The neoproterozoic oxygenation event: Environmental perturbations and biogeochemical cycling. *Earth Sci Rev* 110(1):26–57.
133. Sperling EA, et al. (2015) Statistical analysis of iron geochemical data suggests limited late proterozoic oxygenation. *Nature* 523(7561):451–454.
134. Canfield D (1998) A new model for proterozoic ocean chemistry. *Nature* 396(6710):450–453.
135. Canfield DE, et al. (2008) Ferruginous conditions dominated later neoproterozoic deep-water chemistry. *Science* 321(5891):949–952.
136. Planavsky NJ, et al. (2011) Widespread iron-rich conditions in the mid-Proterozoic ocean. *Nature* 477(7365):448–451.
137. Reinhard CT, et al. (2013) Proterozoic ocean redox and biogeochemical stasis. *Proc Natl Acad Sci USA* 110(14):5357–5362.
138. Anbar AD, Knoll A (2002) Proterozoic ocean chemistry and evolution: A bioinorganic bridge? *Science* 297(5584):1137–1142.
139. Fennel K, Follows M, Falkowski PG (2005) The co-evolution of the nitrogen, carbon and oxygen cycles in the Proterozoic ocean. *Am J Sci* 305(6-8):526–545.
140. Reinhard CT, et al. (2017) Evolution of the global phosphorus cycle. *Nature* 541(7637):386–389.
141. Jelen BI, Giovannelli D, Falkowski PG (2016) The role of microbial electron transfer in the coevolution of the biosphere and geosphere. *Ann Rev Microbiol* 70: 45–62.
142. Robbins LJ, et al. (2016) Trace elements at the intersection of marine biological and geochemical evolution. *Earth Sci Rev* 163:323–348.
143. Gledhill M, Buck KN (2012) The organic complexation of iron in the marine environment: A review. *Front Microbiol* 3:69.
144. Banfield JF, Barker WW, Welch SA, Taunton A (1999) Biological impact on mineral dissolution: Application of the lichen model to understanding mineral weathering in the rhizosphere. *Proc Natl Acad Sci USA* 96(7):3404–3411.
145. Jickells T, et al. (2005) Global iron connections between desert dust, ocean biogeochemistry, and climate. *Science* 308(5718):67–71.
146. Benitez-Nelson CR (2000) The biogeochemical cycling of phosphorus in marine systems. *Earth Sci Rev* 51(1):109–135.
147. Ryan P, Delhaize E, Jones D (2001) Function and mechanism of organic anion exudation from plant roots. *Ann Rev Plant Biol* 52(1):527–560.
148. Berner RA, Canfield DE, et al. (1989) A new model for atmospheric oxygen over phanerozoic time. *Am J Sci* 289(4):333–361.
149. Berner RA (1997) The rise of plants and their effect on weathering and atmospheric $CO_2$. *Science* 276(5312):544–546.
150. Lenton TM, Crouch M, Johnson M, Pires N, Dolan L (2012) First plants cooled the ordovician. *Nat Geosci* 5(2):86–89.
151. Yoon HS, Hackett JD, Ciniglia C, Pinto G, Bhattacharya D (2004) A molecular timeline for the origin of photosynthetic eukaryotes. *Mol Biol Evol* 21(5):809–818.
152. Douzery EJ, Snell EA, Bapteste E, Delsuc F, Philippe H (2004) The timing of eukaryotic evolution: Does a relaxed molecular clock reconcile proteins and fossils? *Proc Natl Acad Sci USA* 101(43):15386–15391.
153. Parfrey LW, Lahr DJ, Knoll AH, Katz LA (2011) Estimating the timing of early eukaryotic diversification with multigene molecular clocks. *Proc Natl Acad Sci USA* 108(33):13624–13629.
154. Shih PM, Matzke NJ (2013) Primary endosymbiosis events date to the later proterozoic with cross-calibrated phylogenetic dating of duplicated atpase proteins. *Proc Natl Acad Sci USA* 110(30):12355–12360.
155. Knoll AH, Javaux EJ, Hewitt D, Cohen P (2006) Eukaryotic organisms in proterozoic oceans. *Philos Trans R Soc Lond B Biol Sci* 361(1470):1023–1038.
156. Javaux E (2011) Early eukaryotes in Precambrian oceans. *Origins and Evolution of Life: An Astrobiological Perspective*, eds Gargaud M, Lopez-Garcia P, Martin H (Cambridge Univ Press, Cambridge, UK), pp 414–449.
157. Logan GA, Hayes JM, Hieshima GB, Summons RE (1995) Terminal Proterozoic reorganization of biogeochemical cycles. *Nature* 376(6535):53–56.
158. Lenton TM, Boyle RA, Poulton SW, Shields-Zhou GA, Butterfield NJ (2014) Co-evolution of eukaryotes and ocean oxygenation in the Neoproterozoic era. *Nat Geosci* 7(4):256–265.
159. Keeling RF, Piper SC, Heimann M (1996) Global and hemispheric $CO_2$ sinks deduced from changes in atmospheric $o_2$ concentration. *Nature* 381(6579):218–221.
160. Ciais P, et al. (2013) Carbon and other biogeochemical cycles. *Climate Change 2013: The Physical Science Basis*. Contribution of Working Group I to the Fifth Assessment Report of the Intergovernmental Panel on Climate Change, eds Stocker T, et al. (Cambridge Univ Press, Cambridge, UK), pp 465–570.
161. Shih PM, et al. (2013) Improving the coverage of the cyanobacterial phylum using diversity-driven genome sequencing. *Proc Natl Acad Sci USA* 110(3):1053–1058.
162. Biller SJ, et al. (2014) Genomes of diverse isolates of the marine cyanobacterium *Prochlorococcus*. *Sci Data* 1:140034.
163. Camacho C, et al. (2009) Blast+: Architecture and applications. *BMC Bioinformatics* 10:421.

**Supporting Information for**
**"Metabolic evolution and the self-organization of ecosystems"**

**R. Braakman*, M.J. Follows, S.W. Chisholm****
***rogierbraakman@gmail.com, ****chisholm@mit.edu**

## SI Text

### Glossary of terms

| Term | Definition | Units |
|---|---|---|
| $a_n^0$ | Specific nutrient affinity | L (g dry weight)$^{-1}$ time$^{-1}$ |
| $\beta$ | Fraction of the cellular carbon flux density that is excreted | unitless, ranges between 0 and 1 |
| $\#C/\#e$ | Efficiency of carbon fixation | carbon atoms electron$^{-1}$ |
| $\Delta_r G$ | Free energy of reaction | kJ mol$^{-1}$ |
| $[E]$ | Enzyme concentration | moles of enzyme (g dry weight)$^{-1}$ |
| $F$ | Faraday constant | $9.6485 \times 10^4$ coulombs mol$^{-1}$ |
| $I$ | Light intensity | μmol photons m$^{-2}$ time$^{-1}$ |
| $K_{M,n}$ | Whole-cell Michaelis constant | moles of $n$ L$^{-1}$ |
| $k^+$ | Rate constant | moles of $n$ (moles of enzyme)$^{-1}$ time$^{-1}$ |
| $\mu$ | Specific growth rate | time$^{-1}$ |
| $\mu_{max}$ | Maximal intrinsic growth rate | time$^{-1}$ |
| $[n]$ | Environmental concentration of nutrient $n$ | moles of $n$ L$^{-1}$ |
| $[n]^*$ | Minimal subsistence concentration of nutrient $n$ | moles of $n$ L$^{-1}$ |
| $P_n$ | Membrane permeability of nutrient $n$ | μm time$^{-1}$ |
| $\phi_{PSII}$ | Quantum efficiency of PSII | electrons photon$^{-1}$ |
| $\Delta\psi$ | Membrane potential | mV |
| $Q_n$ | Mass-normalized cell quota of nutrient $n$ | moles of $n$ (g dry weight)$^{-1}$ |
| $R$ | Gas constant | 8.3145 J K$^{-1}$ mol$^{-1}$ |
| $r_{cell}$ | Cell radius | μm |
| $\sigma_{PSII}$ | Mass-normalized whole-cell PSII absorption cross-section | m$^2$ of PSII (g dry weight)$^{-1}$ |
| $T$ | Temperature | K |
| $v_e$ | Cellular electron flux density | μmol electrons (g dry weight)$^{-1}$ time$^{-1}$ |
| $v_n$ | Nutrient uptake flux density | moles of $n$ (g dry weight)$^{-1}$ time$^{-1}$ |
| $V_{cyt}$ | Mass-normalized cytoplasmic volume | mL (g dry weight)$^{-1}$ |
| $V_{max}$ | Maximal nutrient uptake flux density | moles of $n$ (g dry weight)$^{-1}$ time$^{-1}$ |
| $Z$ | Nutrient charge | unitless |

### Hypotheses for benefits of draining excess reducing power into the environment

Studies of oceanic phytoplankton have led to several hypotheses of why cells may drain excess reducing power into the environment rather than lowering their photosynthetic electron flux. One suggestion is that slow, nutrient-limited growth increases the need for ATP-heavy maintenance metabolism relative to more NAD(P)H-heavy *de novo* biosynthesis, and that the water-water cycle mediated by PTOX allows cells to increase their relative ATP/NAD(P)H supply [1]. Another argument is that low iron concentrations in the open ocean promote the more iron-efficient modified electron flow facilitated by PTOX [2-4], which is consistent with the loss of several iron-sulfur enzymes in the rest of *Prochlorococcus*' metabolic core (Fig. S1). However, neither hypothesis clarifies why *Prochlorococcus* should acquire ATP-*consuming* pathways involved in the excretion of organic carbon prior to innovations in the electron transfer chain that would appear most effective at increasing both iron efficiency and the relative supply of ATP.

Other hypotheses for why a photoautotrophic cell might drain excess reducing power into the environment come from studies on the excretion of organic carbon by heterotrophic microbes. One proposes that excreting organic carbon facilitates a less efficient, but intrinsically faster, mode of ATP production that requires less protein, allowing cells with an abundant energy supply to achieve faster growth by allocating more protein to biosynthesis [5-7]. This is consistent with *Prochlorococcus* using the Entner-Doudoroff (ED) rather than the Emden-Meyerhoff-Parnas (EMP) variant of glycolysis to catabolize glucose as a supplementary energy source

alongside photosynthesis [8], since ED glycolysis has a higher intrinsic rate and lower protein cost than EMP glycolysis [6]. However, *Prochlorococcus* is characterized by a slow growth rate [9,10], and it is unclear why its cells should supplement phototrophy with chemoheterotrophy if the energy supply outpaces the nutrient supply (Fig. 1 in the main text). It is similarly unclear how excreting organic carbon would lower the protein requirement of ATP production during photosynthesis. Another suggestion is that excreting organic carbon and other forms of "energy spilling" (e.g. various enzymatic futile cycles) allow nutrient-limited cells to maintain high energy throughput of their metabolism so they can rapidly 'reignite' growth once limitation is lifted [11,12]. However, while the deeper-branching *Synechococcus* is found throughout the surface oceans and can exhibit rapid blooms in response to nutrient influxes, particularly in coastal regions [13,14], *Prochlorococcus* is restricted to the low nutrient oligotrophic oceans [15-17] and maintains a fairly steady growth rate [18]. Thus, while various hypotheses provide clues about relevant driving forces, they leave us without a completely satisfying explanation for the metabolic evolution of *Prochlorococcus* (Fig. 3 in the main text and surrounding discussion).

**Nutrient uptake and nutrient affinity**

Evidence suggests that the increasing excretion of organic carbon over the course of evolution in *Prochlorococcus* is part of a general trend that increases the cellular metabolic rate, and that this may benefit the uptake of limiting nutrients (see main text for discussion). To understand how metabolic rate and nutrient uptake are related we begin by examining basic principles of nutrient uptake. We can consider nutrient uptake by a cell as the reaction $n \rightleftharpoons n_I$, where $n$ is the nutrient in the environment at concentration $[n]$ and $n_I$ is nutrient $n$ internal to the cell at concentration $[n]_I$. The flux density of nutrient uptake $v_n$ is given by the standard Michaelis-Menten equation:

$$v_n = \frac{V_{max}[n]}{K_{M,n} + [n]} \quad (1)$$

where $V_{max}$ is the maximal saturated uptake rate of the transport reaction and $K_{M,n}$ is the Michaelis constant. Under extreme nutrient-limitation ($[n] << K_{M,n}$) Eq. 1 simplifies to [19]:

$$v_n = V_{max}[n]/K_{M,n} = a_n^0[n] \quad (2)$$

where $a_n^0$ is the specific nutrient affinity. The relationship between $v_n$, $a_n^0$, $V_{max}$, and $K_{M,n}$ is shown visually in Fig. S3. To understand how cellular growth is affected by nutrient-limitation, we can rewrite Eq. 2 as:

$$[n] = v_n/a_n^0 = v_n K_{M,n}/V_{max} \quad (3)$$

The minimal subsistence nutrient concentration $[n]^*$ is the lowest steady-state value of $[n]$ at which cells can achieve net positive growth. Thus, cells can lower their $[n]^*$ through two basic adaptations: increasing their specific affinity $a_n^0$ or decreasing their *required* nutrient flux density $v_n$ (Eq. 3 and Fig. S3). Since the *required* nutrient flux density is given by $v_n = \mu Q_n$ (Eq. 2 in the main text), where $\mu$ is the specific growth rate and $Q_n$ is the mass-normalized cellular quota of nutrient $n$, cells can therefore adapt to nutrient-limitation by lowering $\mu$ and/or $Q_n$ (blue arrows in Fig. S3). Alternatively, since the nutrient affinity is equal to $V_{max}/K_{M,n}$, cells can adapt to nutrient-limitation by increasing $V_{max}$ and/or decreasing $K_{M,n}$, which increases $v_n$ (and thereby $\mu$) *at a given nutrient concentration* (red arrows in Fig. S3). It is the selection for an increasing $V_{max}$ (and thus $a_n^0$) that we argue explains the benefit of increasing metabolic rate under nutrient-limitation, as we discuss next.

**Relating nutrient affinity and metabolic rate**

To understand how metabolic rate affects $V_{max}$ and thereby the minimal subsistence nutrient concentration of cells (Eq. 3), we perform a thought experiment using basic principles of reaction kinetics. The scenario outlined above considers only the initial uptake reaction $n \rightleftharpoons n_I$, but in reality that reaction is part of a large network of reactions (metabolism) that collectively processes the entire conversion from external nutrient to biomass. In principle cells can thus increase the rate of nutrient uptake by increasing the rate of the

downstream metabolic network [19,20], which can be further understood by considering a simplified metabolic network consisting of two reversible reactions:

$$n \rightleftharpoons n_I \quad (4)$$
$$n_I \rightleftharpoons M \quad (5)$$

The reaction rate of reaction 5 (the "downstream metabolic network" that converts nutrient $n$ to biomass building block $M$) is given by the standard reversible Michaelis-Menten equation:

$$v_{n_I \to M} = v^+ - v^- = [E]\frac{k^+ [n]_I/K_{M,n} - k^- [M]/K_{M,M}}{1 + [n]_I/K_{M,n} + [M]/K_{M,M}} \quad (6)$$

Where $v^+$ and $v^-$ are the forward and backward rates, $k^+$ and $k^-$ are the forward and backward rate constants, $[E]$ is the enzyme concentration and $[M]$ is the concentrations of $M$ inside the cell. The Gibbs free energy of reaction of reaction 5 is given by [21,22]:

$$\Delta_r G = -RT \ln\left(\frac{[n]_I K_{M,M} K_{eq}}{[M] K_{M,n}}\right) \quad (7)$$

Where $R$ is the gas constant, $T$ is the temperature, and $K_{eq} = k^+/k^-$ is the equilibrium constant. If we assume that strong environmental nutrient-limitation leads to strong nutrient-limitation of the internal assimilation reaction ($[n]_I << K_{M,n}$) and we make the additional simplifying assumption that enzyme active sites for the backward reaction are also far from saturated ($[M] << K_{M,M}$) we can rewrite Eq. 6 to [21-23]:

$$v_{n_I \to M} = [E]\frac{k^+ [n]_I}{K_{M,n}}\left(1 - e^{\Delta_r G/RT}\right) \quad (8)$$

Eq. 8 allows us to consider how increasing the metabolic rate of cells impacts the nutrient uptake rate. In a closed system, reactions will tend to equilibrate toward a state with no net flux and $\Delta_r G = 0$ [24]. A given starting ratio $[n]_I/[M]$ will thus undergo a more significant decrease for reactions with an intrinsically more negative $\Delta_r G$ (Eq. 7). This same principle holds in open systems, except that there equilibrium is prevented by a steady flux of $n$ in and $M$ out of the system. Thus, in an open system, a reaction with a more negative $\Delta_r G$ (e.g. due to a high value of $K_{eq}$, or coupling the reaction to a more exothermic second reaction) will have a higher intrinsic rate (Eq. 8) and will settle into a steady state with a lower ratio $[n]_I/[M]$ (Eq. 7). But, because the rate of reaction 4 also depends on $[n]_I$, a more negative $\Delta_r G$ for reaction 5 thereby creates a "pull" on reaction 4 by making its $\Delta_r G$ more negative, thus increasing the rate of nutrient uptake into the cell and in turn the overall flux from $n$ to $M$. Comparing the forms of Eq. 8 and Eq. 2, we can see that for a reversible system, $a_n^0$ and $V_{max}$ are given by:

$$a_n^0 = \frac{[E]k^+}{K_{M,n}}\left(1 - e^{\Delta_r G/RT}\right) \quad (9)$$

$$V_{max} = [E]k^+\left(1 - e^{\Delta_r G/RT}\right) \quad (10)$$

In real systems, nutrient transport (rxn 4) is often an active process. Indeed, active transport becomes essential under nutrient-limitation as the following examples show, which thus slightly modifies the considerations above. Active transport drives up $[n]_I$ relative to $[n]$, thereby driving forward downstream metabolism (rxn 5) without the need to increase the energetic driving force on the latter. However, active transport also requires an energetic driving force, which scales with the natural log of the ratio of internal and external nutrient concentrations [25]. Active transport thus follows the same basic principle as stimulating passive uptake by energetically driving downstream metabolism, with the biggest difference being where in the network the driving force is applied. Moreover, the energetic driving of uptake and of downstream reactions can work in tandem to increase the overall rate of nutrient assimilation. This is illustrated using the Gibbs free energy for the nutrient transport reaction (rxn 4), which is given by [25]:

$$\Delta_r G = RT \ln\left(\frac{[n]_I}{[n]}\right) + ZF\Delta\psi \quad (11)$$

where $Z$ is the unit charge of the transported nutrient, $F$ is the Faraday constant and $\Delta\psi$ is the membrane potential (mV). Thus, internally accumulating nutrients (first term in right hand side of Eq. 11) to commonly assumed physiological concentrations of 1 mM from near-vanishing background levels (<0.1 nM), as is the case for N, P & Fe in much of the oligotrophic oceans [26], carries a free energy cost $\Delta_r G$ > 40 kJ/mol. This cost is then combined with the free energy cost of transport against the electric gradient (second term in right hand side of Eq. 11) to give the total free energy cost. For example, assuming a typical bacterial membrane potential of 120 mV (negative inside) [25], the total free energy cost of transporting phosphate ($HPO_4^{2-}$, Z = -2 in seawater of pH = 8) is $\Delta_r G$ > 63 kJ/mol. By comparison, at pH=7.5 and an ionic strength of 0.5 M the hydrolysis of ATP (ATP + H2O → ADP + $P_i$) has a free energy of reaction of $\Delta_r G$ = –44.8 kJ/mol if all reactants have a 1 mM concentration [27], which is thus insufficient to allow any significant phosphate uptake in the oligotrophic oceans using the assumptions above. In the same scenario, accumulating phosphate to only 0.01 mM instead of 1 mM lowers the total free energy cost of transport from to $\Delta_r G$ > 52 kJ/mol, while increasing the ATP/ADP ratio to 10 (in addition to lowering $[P_i]$ to 0.01 mM) lowers the free energy of ATP hydrolysis to $\Delta_r G$ = –61.9 kJ/mol [27], together allowing phosphate transport to proceed in the net forward direction under conditions like those in the oligotrophic oceans.

Further, applying an energetic driving force solely on the uptake reaction itself may not always be the most efficient solution. For example, under N-limitation the uptake and assimilation of ammonia ($NH_4^+$) can lead to a futile cycle, as its conjugate base ($NH_3$) diffuses passively out of the cell, and this loss rate increases with the concentration gradient [28]. It is therefore thought that N-limited cells will poise the internal $NH_4^+$ concentration to the minimal viable value to limit futile cycling [29], which is helped by increasing the energetic driving of downstream reactions. This can be understood by examining the Glutamine Synthetase reaction (Glutamate + $NH_3$ + ATP ⇌ Glutamine + ADP + $P_i$), the central highway for nitrogen into metabolism [25]. At pH=7.5 and an ionic strength of 0.5 M and again using commonly assumed physiological concentrations of 1 mM for all reactants, glutamine synthesis has a $\Delta_r G$ of –15.4 kJ/mol [27], making it essentially irreversible. However, an internal $NH_4^+$ concentration of 1 mM would lead to high levels of futile transport cycling as can be seen by comparing the fluxes for nitrogen assimilation (Eq. 2 in the main text) and diffusive $NH_3$ loss [29]:

$$\upsilon_N = \mu Q_N \quad (12)$$

$$\upsilon_{N,loss} = 3P_{NH_3}([NH_3]_{in} - [NH_3]_{ex})V_{cyt}/r_{cell} \quad (13)$$

where $P_{NH_3}$ is the membrane permeability for $NH_3$ (μm time$^{-1}$), $[NH_3]_{in,out}$ are the internal and external concentrations of $NH_3$ (moles L$^{-1}$), $V_{cyt}$ is the mass-normalized cytoplasmic volume (mL (g of dry weight)$^{-1}$), $r_{cell}$ is the cell radius (μm), $Q_N$ is the mass-normalized cell quota of nitrogen (moles of $N$ (g of dry weight)$^{-1}$) and μ is the specific growth rate (time$^{-1}$). (For consistency we have modified the equations of Ref. [29] to give fluxes in units of (g of dry weight)$^{-1}$ rather than L$^{-1}$.) If we assume ammonia is actively taken up as $NH_4^+$ to an internal concentration $[NH_4^+]_{in}$ = 1 mM, and we further assume an internal pH of 7.5, then $[NH_3]_{in}$ = 18 μM (the pKa of ammonia is 9.25 at room temperature). Further assuming a *Prochlorococcus* cell radius of $r_{cell}$ = 0.3 μm, a typical bacterial value for $V_{cyt}$ of 2 mL (g of dry weight)$^{-1}$ [29], and a relatively conservative $P_{NH_3}$ of 10 μm/s (values up to 2000 μm/s have been measured [29]), then if $[NH_3]_{ex}$ is near-vanishing [26] the diffusive $NH_3$ loss would be 3.6 μmole (g of dry weight)$^{-1}$ s$^{-1}$. Meanwhile, a *Prochlorococcus* cell with a $Q_N$ of ~7 mmole N (g of dry weight)$^{-1}$ (based on an N content of ~0.1 g (g of dry weight)$^{-1}$ [30] and a molar mass of N of 14 g mole$^{-1}$), growing near its maximal growth rate of ~0.7 day$^{-1}$ would have a N assimilation flux of 57 nmole (g of dry weight)$^{-1}$ s$^{-1}$. The loss flux of ammonia through passive diffusion would thus be two orders of magnitude higher than the assimilation flux, leading to very high levels of futile transport cycling.

Keeping all other reactant concentrations fixed and lowering $[NH_4^+]_{in}$ to 1 μM and thereby $[NH_3]_{in}$ to 0.018 μM would lower the passive diffusive loss rate of $NH_3$ to 3.6 nmole (g of dry weight)$^{-1}$ s$^{-1}$, well below the assimilation flux calculated above. However, the net flux of the glutamine synthetase reaction would run in

reverse with a $\Delta_r G$ of +1.7 kJ/mol [27], creating a kinetic bottleneck in the assimilation of ammonia. As before, increasing the ATP/ADP ratio from 1 to 10 while lowering $[P_i]$ to 0.01 mM would lower the $\Delta_r G$ below 0 and drive glutamine synthesis, and thereby ammonia assimilation, forward in the oligotrophic oceans.

We note that cells using nitrate ($NO_3^-$) as their nitrogen source face an intermediary scenario compared to the examples of phosphate or ammonia uptake. Nitrate has a charge Z = –1 at pH = 8, resulting in a free energy cost of uptake $\Delta_r G$ > 51.5 kJ/mol when accumulating it to an internal concentration of 1 mM from external levels of <0.1 nM [26]. This is lower than the free-energy cost of uptake for phosphate (which has a higher cost due to its charge of Z = –2), thus requiring less energetic driving than the latter. However, nitrate uptake again faces the costs of futile transport cycling, since it is first reduced to $NH_4^+$ before being assimilated via glutamine synthetase. Passive loss of $NH_3$ would thus also be significant during growth on nitrate in the oligotrophic oceans, unless $[NH_4^+]_{in}$ is poised at the minimal viable value [29], again requiring greater energetic driving (through an increased ATP/(ADP×$P_i$) ratio) of glutamine synthesis.

The examples above illustrate the importance of increasing the ATP/(ADP×$P_i$) ratio to drive forward nutrient assimilation in the oligotrophic oceans. However, increasing the ATP/(ADP×$P_i$) ratio also makes ATP synthesis more thermodynamically uphill, which therefore requires a greater proton motive force, and thus for photosynthetic cells a greater photosynthetic electron flux [20].

**Increasing metabolic rate and the benefits of excreting organic carbon**

The preceding sets the stage for understanding why excreting organic carbon may be beneficial to cells with a plentiful energy supply. Cells can drive up their ATP/ADP ratio by increasing the ATP supply rate, but to maintain stead-state balance must then also increase their ATP consumption rate [11,20]. A major sink of ATP in a photosynthetic cell is $CO_2$-fixation. But, cells are limited in the carbon-flux density then can accommodate, and this upper limit is proportional to both the maximal cellular carbon density (i.e. the maximal $Q_C$) and the growth rate $\mu$. This upper limit on the carbon flux density is thus lower under strong nutrient-limitation, which favors slow growth (Eq. 3), but in principle exists for any $\mu$. We thus argue that excretion of organic carbon allows cells to increase their metabolic rate above the point where the carbon flux exceeds the growth requirement. This can be further understood by expanding Eq. 3 using several assumptions. We assume that under nutrient limitations cells take up limiting nutrient $n$ with maximal efficiency, but can be inefficient with all non-limiting resources. In other words, if we further assume that biomass has an elemental stoichiometry $Q_C/Q_n$, then cells must fix $CO_2$ at a rate *at least* equivalent to $v_n(Q_C/Q_n)$, but can in principle fix carbon at higher rates and excrete the excess carbon flux. We further assume that the fraction of fixed carbon that is excreted or respired is $\beta$, which falls in a range ($0<\beta<1$), and that the efficiency of $CO_2$-fixation is $\#C/\#e$. The carbon/electron flux ratio $\#C/\#e$ depends on the oxidation state of the carbon source, biomass and excreted carbon. For photosynthetic cells fixing $CO_2$ and producing biomass and excreted carbon at an average oxidation state of $CH_2O$, $\#C/\#e$ is 1/4 (i.e. $CO_2 + 4\ H^+ + 4\ e^- \rightleftharpoons CH_2O + H_2O$). Photoprotective mechanisms such as PTOX (Fig. S1) that direct electron flux out of the electron transport chain prior to carbon-fixation act to lower $\#C/\#e$. Under these assumptions, the nutrient, carbon and electron flux densities of nutrient-limited cells are related through:

$$v_n = \frac{Q_n}{Q_C} v_e (\#C/\#e)(1-\beta) \tag{14}$$

Finally, we can combine Equations 3, 9 and 14 to give:

$$[n] = \frac{K_{M,n}}{[E]k^+} \times \frac{v_n}{(1-e^{\Delta_r G/RT})} = \frac{K_{M,n}}{[E]k^+} \times \frac{Q_n}{Q_C} \times \frac{v_e(\#C/\#e)(1-\beta)}{(1-e^{\Delta_r G/RT})} \tag{15}$$

Eq. 15 describes how selection to lower $[n]^*$ shapes cellular features. As discussed earlier, selection to lower $[n]^*$ favors decreases in $v_n$ and $\Delta_r G$ (Equations 3, 9 and 10), and as we just argued decreases in $\Delta_r G$ are achieved through an increased electron flux. But an increased electron flux also leads to an increased carbon flux, which in turn acts to drive up $[n]^*$. Therefore, selection to lower $[n]^*$ should simultaneously favor an increasing $v_e/v_n$ and an increasing excretion of organic carbon, exactly as we observe for the evolution of *Prochlorococcus*. See main text for further discussion.

## References


1. Behrenfeld MJ, Prasil O, Babin M, Bruyant F (2004) In search of a physiological basis for covariations in light-limited and light-saturated photosynthesis. *J Phycol* 40(1):4-25.
2. Bailey S et al. (2008). Alternative photosynthetic electron flow to oxygen in marine *Synechococcus*. *Biochim Biophys Acta - Bioenergetics* 1777(3):269-276.
3. Strzepek RF, Harrison PJ (2004). Photosynthetic architecture differs in coastal and oceanic diatoms. *Nature*, 431(7009):689-692.
4. Cardol P et al. (2008) An original adaptation of photosynthesis in the marine green alga *Ostreococcus*. *Proc Natl Acad Sci USA* 105(22):7881-7886.
5. Molenaar D, van Berlo R, de Ridder D, Teusink B (2009). Shifts in growth strategies reflect tradeoffs in cellular economics. *Mol Syst Biol* 5(1):323.
6. Flamholz A, Noor E, Bar-Even A, Liebermeister W, Milo R (2013). Glycolytic strategy as a tradeoff between energy yield and protein cost. *Proc Natl Acad Sci USA* 110(24) 10039-10044.
7. Basan M et al. (2015) Overflow metabolism in *Escherichia coli* results from efficient proteome allocation. *Nature*, 528(7580):99-104.
8. Chen X et al. (2016) The entner–doudoroff pathway is an overlooked glycolytic route in cyanobacteria and plants. Proc Natl Acad Sci USA pp. 5441–5446.
9. Moore LR, Goericke R, Chisholm SW (1995) Comparative physiology of *Synechococcus* and *Prochlorococcus*: influence of light and temperature on growth, pigments, fluorescence and absorptive properties. *Mar Ecol Prog Ser* 116(1):259-275.
10. Partensky F, Blanchot J, Lantoine F, Neveux J, Marie D (1996) Vertical structure of picophytoplankton at different trophic sites of the tropical northeastern atlantic ocean. Deep Sea Research Part I: Oceanographic Research Papers 43(8):1191–1213.
11. Neijssel OM, Tempest DW (1976) The role of energy-spilling reactions in the growth of *Klebsiella aerogenes* NCTC 418 in aerobic chemostat culture. *Arch Microbiol* 110(2-3):305-311.
12. Russell JB, Cook GM (1995). Energetics of bacterial growth: balance of anabolic and catabolic reactions. *Microbiol Rev*, 59(1), 48-62.
13. Waterbury JB, Watson SW, Valois FW, Franks DG (1986) Biological and ecological characterization of the marine unicellular cyanobacterium synechococcus. Can Bull Fish Aquat Sci 214(71):120.
14. Hunter-Cevera KR et al. (2016) Physiological and ecological drivers of early spring blooms of a coastal phytoplankter. Science 354(6310):326–329.
15. Partensky F, Hess WR, Vaulot D (1999) Prochlorococcus, a marine photosynthetic prokaryote of global significance. *Microbiol Mol Biol Rev* 63(1):106-127.
16. Flombaum P et al. (2013) Present and future global distributions of the marine Cyanobacteria Prochlorococcus and Synechococcus. *Proc Natl Acad Sci USA* 110(24):9824-9829.
17. Scanlan DJ et al. (2009) Ecological genomics of marine picocyanobacteria. *Microbiol Mol Biol Rev* 73(2):249-299.
18. Ribalet F et al. (2015) Light-driven synchrony of prochlorococcus growth and mortality in the subtropical pacific gyre. Proceedings of the National Academy of Sciences 112(26):8008–8012.
19. Button DK (1991). Biochemical basis for whole-cell uptake kinetics: specific affinity, oligotrophic capacity, and the meaning of the Michaelis constant. *Appl Environ Microbiol* 57(7):2033-2038.
20. Harder W, Dijkhuizen L (1983) Physiological responses to nutrient limitation. Ann Rev Microbiol 37(1):1–23
21. Beard DA, Qian H (2007) Relationship between thermodynamic driving force and one-way fluxes in reversible processes. *PLOS ONE* 2(1):e144.
22. Flamholz A, Noor E, Bar-Even A, Liebermeister W, Milo R (2013). Glycolytic strategy as a tradeoff between energy yield and protein cost. *Proc Natl Acad Sci USA* 110(24):10039-10044.
23. Liebermeister W, Uhlendorf J, Klipp E (2010). Modular rate laws for enzymatic reactions: thermodynamics, elasticities and implementation. *Bioinformatics* 26(12):1528-1534.
24. Atkins PW (1994) Physical Chemistry (Oxford University Press)
25. Lengeler JW, Drews G, Schlegel HG, eds. (1999) Biology of the Prokaryotes. (Thieme).
26. Moore C et al. (2013) Processes and patterns of oceanic nutrient limitation. Nat Geosci 6(9):701–710
27. Calculations were done using the Equilibrator (*equilibrator.weizmann.ac.il*): Noor, Elad, et al. "An integrated open framework for thermodynamics of reactions that combines accuracy and coverage." *Bioinformatics* 28.15 (2012): 2037-2044.
28. Kleiner D (1985) Bacterial ammonium transport. FEMS Microbiology Letters 32(2):87–100
29. Boogerd FC et al. (2011) Amtb-mediated nh3 transport in prokaryotes must be active and as a consequence regulation of transport by glnk is mandatory to limit futile cycling of nh 4+/nh 3. FEBS letters 585(1):23–28
30. Heldal, M., et al. (2003) Elemental composition of single cells of various strains of marine *Prochlorococcus* and *Synechococcus* using X-ray microanalysis. Limnol Oceanograph 48.5 1732-1743.

## SI Figures

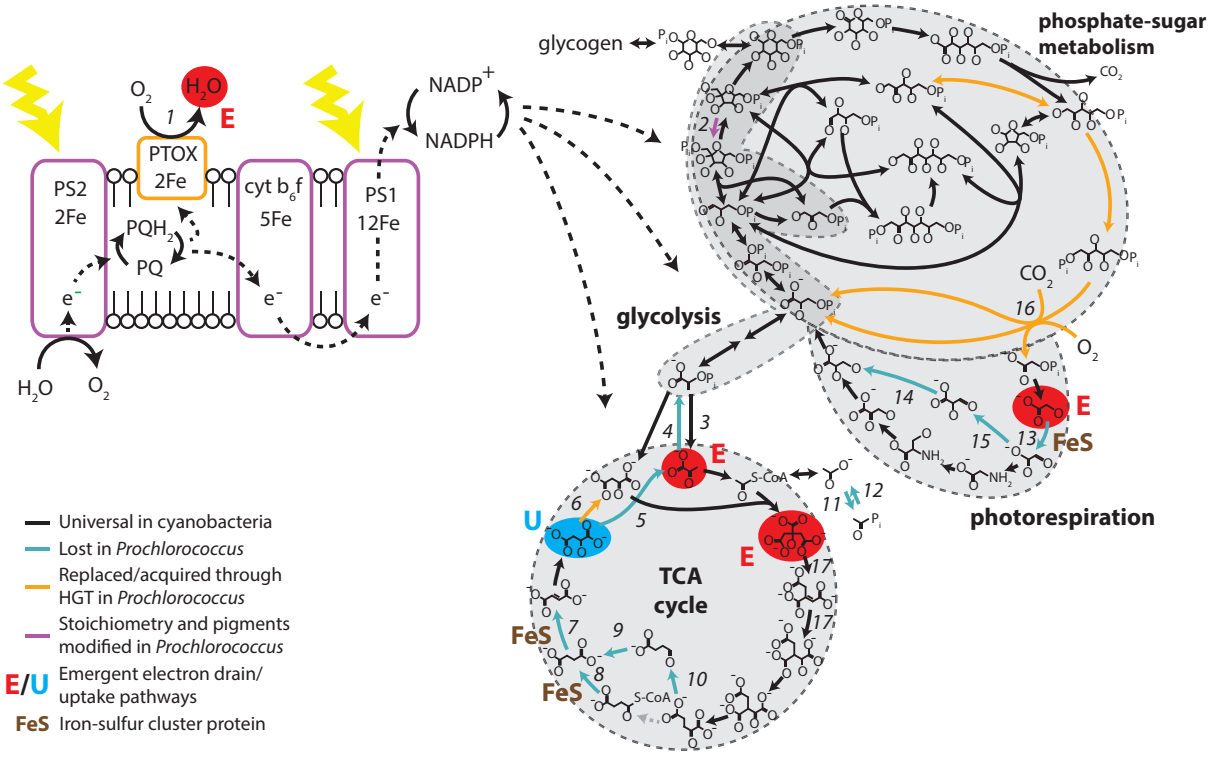


**Figure S1.** Details of the changes in the photosynthetic machinery (left panel) and metabolic core (right panel) of *Prochlorococcus* during its evolutionary divergence (Fig. 3 of main text) from a universal cyanobacterium (black). The photosystems of *Prochlorococcus* (purple) have an altered set of accessory pigments [1-4] and the PSII:Cyt $b_6f$:PSI ratio increases along its phylogeny [5,6]. The photosynthetic electron transport chain of the LLI and HL clades further contains the Plastoquinol Terminal Oxidase (PTOX) (Table S1) as indicated by the orange box. Within core carbohydrate metabolism, key genes are gained and lost as indicated by blue and yellow lines (Table S1). Iron-sulfur cluster enzymes are highlighted in brown. Red circles indicate putative redox safety valves, including those excreting pyruvate, glycolate and citrate or isocitrate, while the blue circle indicates a putative uptake pathway for malate. We suspect citrate rather than isocitrate is excreted because under iron-limitation or oxidative stress aconitase (two-step reaction 17 converting citrate to isocitrate) is post-translationally converted to the iron regulatory protein (IRP) [7], which may lead to accumulation of citrate. Enzyme names of numbered reactions are shown in Table S1 and Fig. S2.


1. Bibby TS, Nield J, Partensky F, Barber J (2001) Oxyphotobacteria: antenna ring around photosystem I. *Nature*, 413(6856):590-590.
2. Scanlan DJ et al. (2009) Ecological genomics of marine picocyanobacteria. *Microbiol Mol Biol Rev* 73(2):249-299.
3. Bibby TS, Mary I, Nield J, Partensky F, Barber J (2003). Low-light-adapted *Prochlorococcus* species possess specific antennae for each photosystem. *Nature*, 424(6952):1051-1054.
4. Chisholm SW et al. (1988) A novel free-living prochlorophyte abundant in the oceanic euphotic zone. *Nature* 334:340-343.
5. Goericke R, Repeta DJ (1992) The pigments of *Prochlorococcus marinus*: The presence of divinylchlorophyll a and b in a marine procaryote. *Limnol Oceanogr* 37(2):425-433.
6. Zorz JK et al. (2015). The RUBISCO to photosystem II ratio limits the maximum photosynthetic rate in picocyanobacteria. *Life* 5(1):403-417.
7. Pantopoulos K, Hentze MW (1995) Rapid responses to oxidative stress mediated by iron regulatory protein. *EMBO J* 14(12):2917.

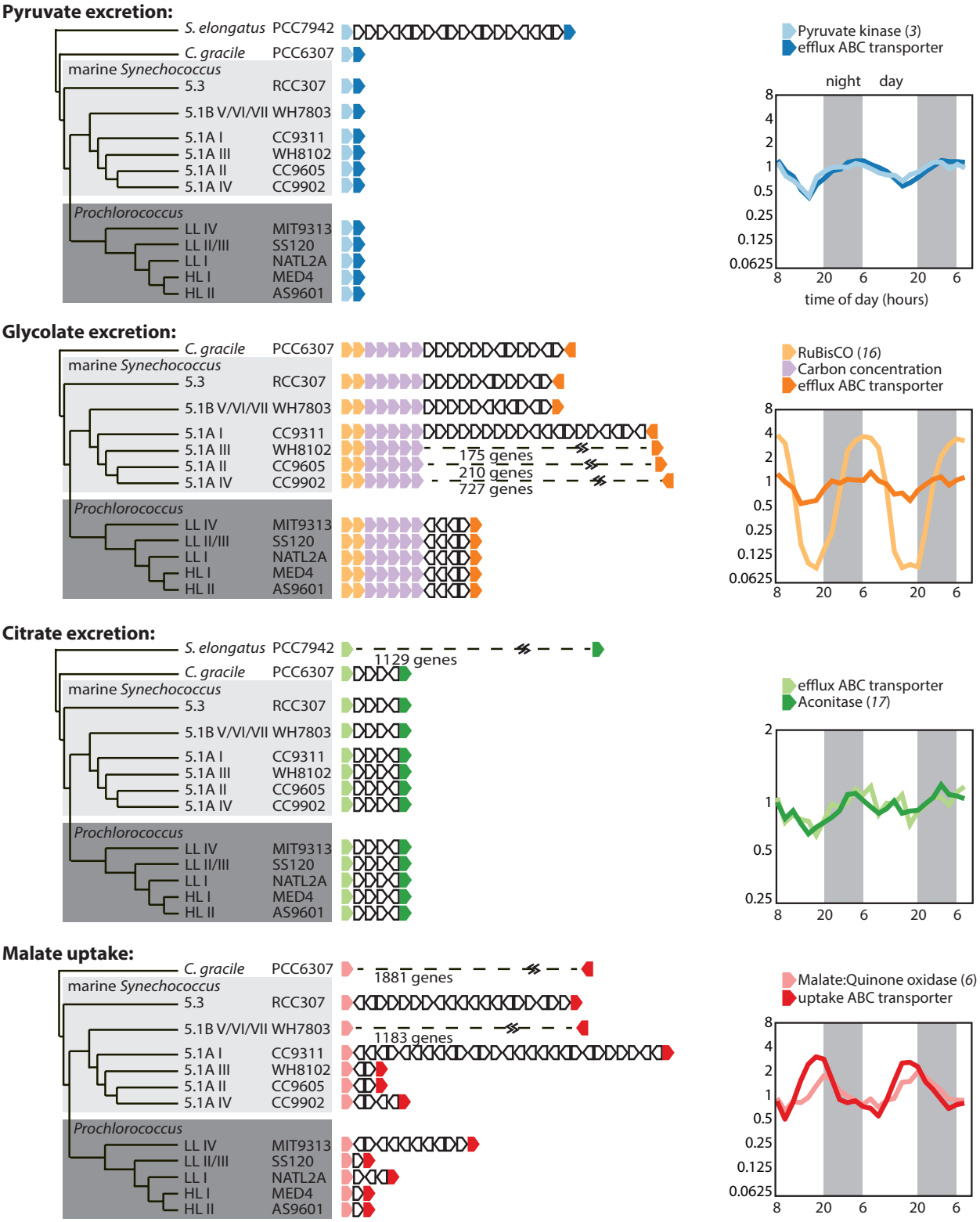


**Figure S2.** Genomic evolution and expression of transport pathways in *Prochlorococcus*. Chromosomal location of key metabolic genes and ABC transporters are shown along the *Prochlorococcus* phylogeny (left panel). In some plots only *Cyanobium gracile* and marine picocyanobacteria are shown because the corresponding metabolic genes are absent in other cyanobacteria (Table S1). Color-coded names of genes are shown on the right, and gene numbers are as in Fig. S1. Changes in the relative transcript levels of genes (log-fold changes in mRNA number) in *Prochlorococcus* MED4 (HLI clade) over a diel L:D cycle [redrawn from Ref. 1] are shown on the right.

1. Zinser ER et al. (2009) Choreography of the transcriptome, photophysiology, and cell cycle of a minimal photoautotroph, Prochlorococcus. *PLoS One* 4(4):e5135

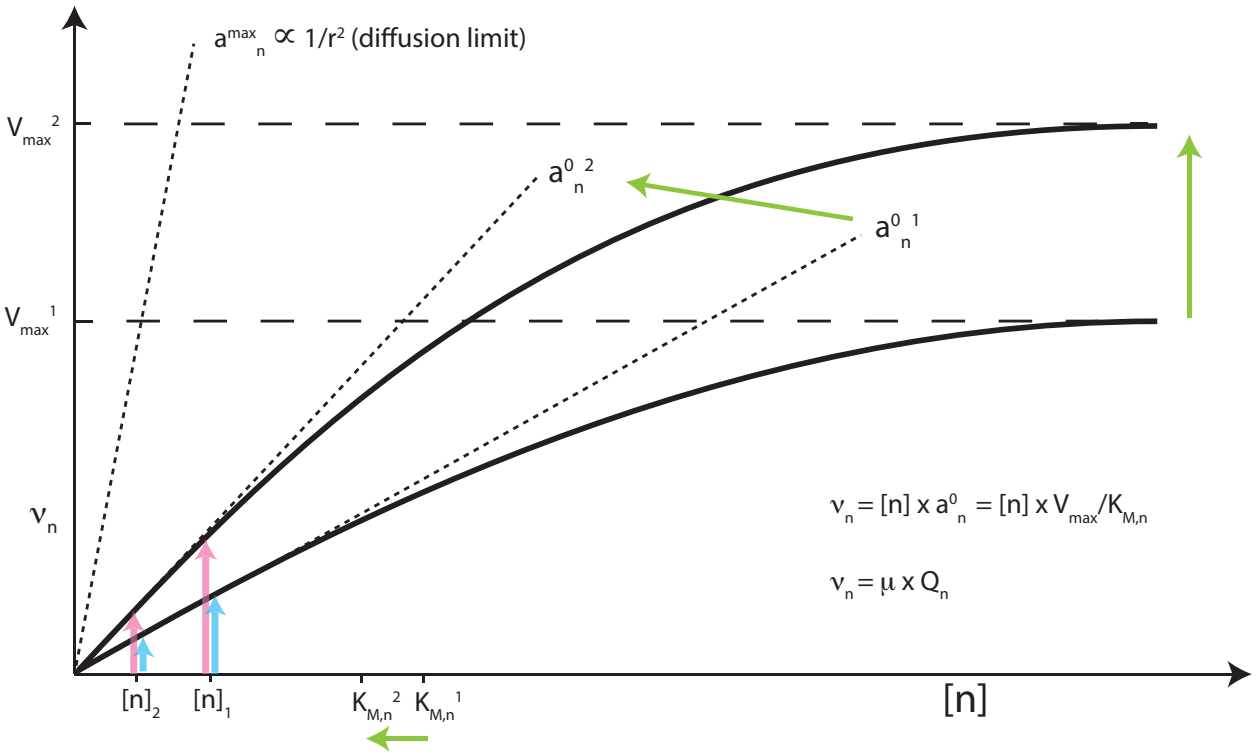


**Figure S3.** Kinetics of nutrient uptake (based on Ref. [1]). The Y-axis is the nutrient uptake rate $v_n$ and the X-axis is nutrient concentration $[n]$. Dotted lines indicate the specific affinity $a_n^0$ and the upper (diffusion) limit on the specific affinity $a_n^{max}$. Dashed lines indicate the maximal saturated uptake rate $V_{max}$. The Michaelis constant $K_{M,n}$ is the nutrient concentration at which $v_n = 1/2\, V_{max}$. Equations show the relationships between $v_n$, $a_n^0$, $V_{max}$ and $K_{M,n}$, and between $v_n$, $\mu$ and $Q_n$. For a fixed nutrient affinity, cells can lower their minimal subsistence nutrient concentration by lowering their *required* nutrient flux $v_n$ (blue arrows). Cells can increase $v_n$ at any nutrient concentration by increasing $a_n^0$ (red arrows), which is achieved by increasing $V_{max}$ and/or decreasing $K_{M,n}$ (green arrows), providing a second route to lowering the minimal subsistence nutrient concentration.

1. Button DK (1991). Biochemical basis for whole-cell uptake kinetics: specific affinity, oligotrophic capacity, and the meaning of the Michaelis constant. *Appl Environ Microbiol* 57(7):2033-2038

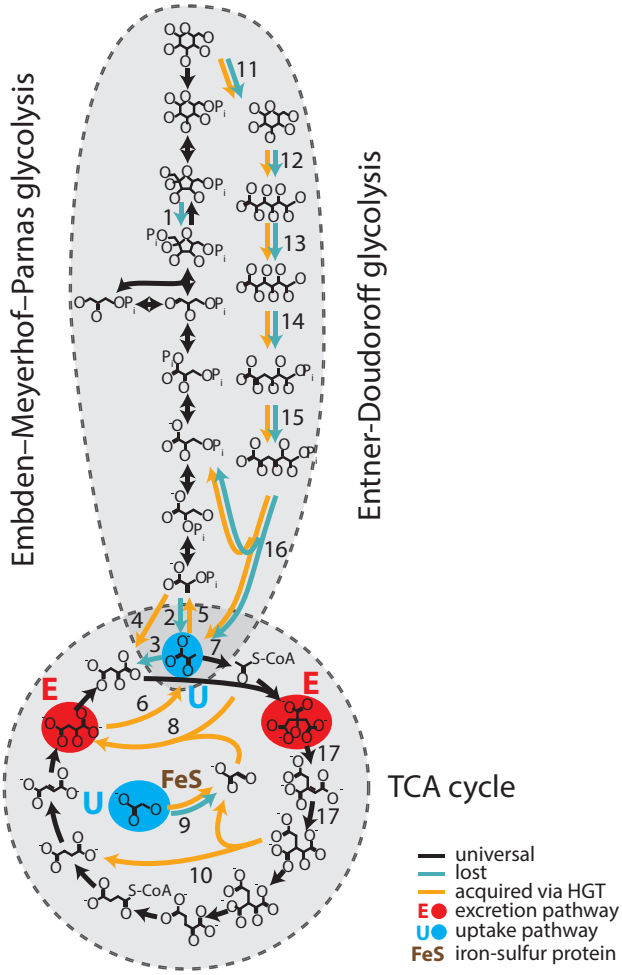


**Figure S4.** Details of the changes in the core metabolism of SAR11 over the course of its evolution. Key genes are gained and lost as indicated by the blue and yellow lines (Table S2). Red dots indicate putative redox outlets that excrete malate and citrate or isocitrate, and blue dots indicate putative uptake pathways for glycolate and pyruvate. As in *Prochlorococcus* we suspect that citrate rather than isocitrate is excreted because aconitase doubles as the iron-regulatory protein [1] (Fig. S1). Enzyme names of numbered reactions are shown in Table S2 and Figure S5.

1. Pantopoulos K, Hentze MW (1995) Rapid responses to oxidative stress mediated by iron regulatory protein. *EMBO J* 14(12):2917.

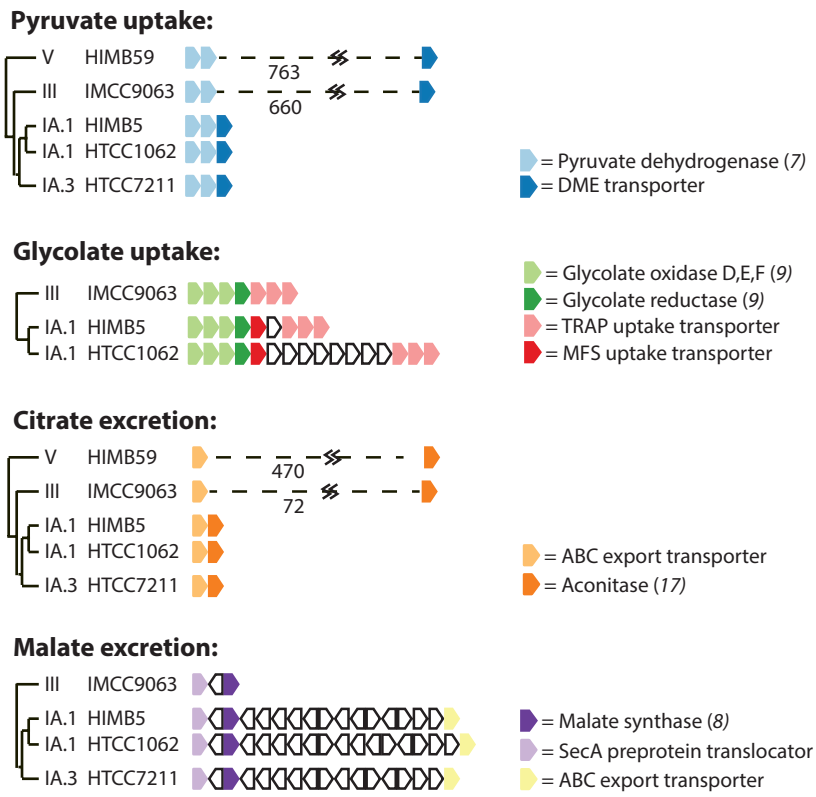


**Figure S5.** Genomic evolution of transport pathways in SAR11. Chromosomal location of key metabolic genes and ABC transporters are shown along the *Prochlorococcus* phylogeny. In some plots SAR11 group V was excluded because it lacks the relevant metabolic genes (Table S2). Color-coded names of genes are shown below each plot, and gene numbers are as in Fig. S2. Here a variety of transporters are involved. The drug/metabolite (DME) transporter family (pyruvate pathway) is implicated in both export [1] and uptake [2], and in shuttling electrons from the cytoplasm to the periplasm under oxidate stress [3,4]. Major Facilitator Superfamily (MFS) uptake transporters and Tripartite ATP-independent periplasmic (TRAP) uptake transporters (glycolate pathway) both depend on proton motive force rather than ATP-hydrolysis to drive transport [5,6]. The SecA transporter is part of the Sec protein translocation system [7], which in *E. coli* contains a plug that prevents transfer of small metabolites [8], but in eukaryotes it is permeable to them [9-11]. We also observe an ABC transporter exclusive to the IA clade (malate pathway).


1. Jack DL, Yang NM, Saier MH (2001). The drug/metabolite transporter superfamily. *Eur J Biochem* 268(13):3620-3639
2. Tucker AM, Winkler HH, Driskell LO, Wood DO (2003). S-Adenosylmethionine transport in Rickettsia prowazekii. *J Bacteriol* 185(10):3031-3035.
3. Ohtsu I et al. (2010) The L-cysteine/L-cystine shuttle system provides reducing equivalents to the periplasm in Escherichia coli. *J Biol Chem* 285(23):17479-17487.
4. Ohtsu I et al. (2015) Uptake of L-cystine via an ABC transporter contributes defense of oxidative stress in the L-cystine export-dependent manner in Escherichia coli. *PLOS ONE* 10(4):e0120619.
5. Pao SS, Paulsen IT, Saier MH (1998) Major facilitator superfamily. *Microbiol Mol Biol Rev* 62(1):1-34.
6. Kelly DJ, Thomas GH (2001). The tripartite ATP-independent periplasmic (TRAP) transporters of bacteria and archaea. *FEMS Microbiol Rev* 25(4):405-424.
7. Driessen AJ, Nouwen N (2008. Protein translocation across the bacterial cytoplasmic membrane. *Annu Rev Biochem* 77:643-667.
8. Park E, Rapoport TA (2011) Preserving the membrane barrier for small molecules during bacterial protein translocation. *Nature* 473(7346):239-242.
9. Heritage D, Wonderlin WF (2001) Translocon pores in the endoplasmic reticulum are permeable to a neutral, polar molecule. *J Biol Chem* 276(25):22655-22662.
10. Roy A, Wonderlin WF (2003) The permeability of the endoplasmic reticulum is dynamically coupled to protein synthesis. *J Biol Chem* 278(7):4397-4403.
11. Le Gall S, Neuhof A, Rapoport TA (2004). The endoplasmic reticulum membrane is permeable to small molecules. *Mol Biol Cell* 15(2):447-455.

## SI Tables

**Table S1. Distribution of core metabolic genes across cyanobacteria highlights the remodeling of the metabolic core (Fig. S1 & Fig. 3 in the main text) during the evolution of marine picocyanobacteria as they diverged from their ancestors**

| | | | Reaction/enzyme* (genomic abundance) | | | | | | | | | | | | | |
|---|---|---|---|---|---|---|---|---|---|---|---|---|---|---|---|---|
| **Clade** | **Number of Genomes** | | **1** | **2** | **4** | **5** | **6** | **7** | **8** | **9** | **10/15[a]** | **11** | **12** | **13** | **14** | **18** |
| | | | | | | | | | | | | | | | | |
| Cyanobacteria | **56** | | | | | | | | | | | | | | | |
| All other groups | 53 | | 12 | 44 | 53 | 53 | 0 | 52[b] | 43 | 51 | 52 | 48 | 34 | 53 | 23 | 17 |
| *Synechococcus elongatus* | 2 | | 0 | 2 | 2 | 2 | 0 | 0 | 0 | 0 | 0 | 2 | 0 | 2 | 0 | 2 |
| *Cyanobium gracile* | 1 | | 0 | 0 | 1 | 1 | 1 | 0 | 0 | 0 | 0 | 1 | 1 | 1 | 0 | 1 |
| | | | | | | | | | | | | | | | | |
| Marine *Synechococcus* | **15** | | | | | | | | | | | | | | | |
| Sub-cluster 5.2 | 3 | | 0 | 0 | 3 | 2 | 3 | 1[b] | 0 | 0 | 2 | 3 | 3 | 3 | 3 | 1 |
| Sub-cluster 5.3 | 1 | | 0 | 0 | 0 | 0 | 1 | 0 | 0 | 1 | 0 | 0 | 1 | 1 | 1 | 1 |
| Sub-cluster 5.1B | 5 | | 0 | 0 | 0 | 0 | 5 | 0 | 0 | 1 | 0 | 3 | 5 | 5 | 4 | 5 |
| Sub-cluster 5.1A | 6 | | 3 | 0 | 0 | 0 | 6 | 4[b] | 0 | 1 | 1 | 2 | 6 | 6 | 6 | 1 |
| | | | | | | | | | | | | | | | | |
| *Prochlorococcus* | **41** | | | | | | | | | | | | | | | |
| LLIV | 5 | | 0 | 0 | 0 | 0 | 5 | 5[b] | 0 | 0 | 0 | 0 | 0 | 5 | 5[c] | 0 |
| LLII-III | 10 | | 0 | 0 | 0 | 0 | 10 | 6[b] | 0 | 0 | 0 | 0 | 0 | 0 | 10[c] | 0 |
| LLI | 4 | | 4 | 0 | 0 | 0 | 4 | 0 | 0 | 0 | 0 | 0 | 0 | 0 | 4[c] | 0 |
| HLI | 3 | | 2 | 0 | 0 | 0 | 2 | 0 | 0 | 0 | 0 | 0 | 0 | 0 | 0 | 0 |
| HLII | 19 | | 19 | 0 | 0 | 0 | 19 | 1[b] | 0 | 0 | 0 | 0 | 0 | 0 | 0 | 0 |

***Enzyme names (see Fig. S1):*** 1 – Plastoquinol Terminal Oxidase (PTOX), 2 – 6-phosphofructokinase, 4 – phosphoenolpyruvate synthase, 5 – malic enzyme, 6 – malate:quinone oxidoreductase (MQO), 7 – succinate dehydrogenase (A,B,C subunits), 8 – succinyl-CoA synthetase, 9 – succinate-semialdehyde dehydrogenase, 10 – 2-oxoglutarate decarboxylase, 11 – acetate kinase, 12 – acetylphosphatase, 13 – 2-glycolate oxidase (D,E,F subunits), 14 – tartronate semialdehyde reductase, 15 – glyoxylate carboligase, 18 – catalase (KatG)

***Notes:*** [a] During our analysis we realized that previous experimental studies on the TCA cycle and photorespiration in cyanobacteria implicated the same gene as catalyzing reactions 10 & 15 [1,2], suggesting that both functions are performed by a promiscuous enzyme. [b] It has previously been noted that in marine picocyanobacteria carrying this 3-subunit enzyme it is a homologue acquired from proteobacteria, that potentially catalyzes the reaction in the opposite direction [3,4]. [c] The presence of this gene in many strains lacking the gene for reaction 15, as well as its absence in freshwater picocyanobacteria, suggests loss prior to reacquisition and involvement in a different function in marine picocyanobacteria.


1. Zhang S, Bryant DA (2011) The tricarboxylic acid cycle in cyanobacteria. *Science* 334(6062):1551-1553.
2. Eisenhut M (2008) The photorespiratory glycolate metabolism is essential for cyanobacteria and might have been conveyed endosymbiontically to plants. *Proc Natl Acad Sci USA* 105(44):17199-17204.
3. Kettler GC et al. (2007) Patterns and implications of gene gain and loss in the evolution of Prochlorococcus. *PLoS Genet* 3(12):e231.
4. Dufresne A et al. (2003) Genome sequence of the cyanobacterium Prochlorococcus marinus SS120, a nearly minimal oxyphototrophic genome. *Proc Natl Acad Sci USA 100*(17):10020-10025.

**Table S2. Distribution of core metabolic genes across SAR11 sub-groups highlights the remodeling of the metabolic core (Fig. S4 & Fig. 5 in the main text) during the evolution of the groups dominating the oligotrophic surface oceans as they diverged from their ancestors**

| | | | Reaction/enzyme* (genomic abundance) | | | | | | | | | | | | | | | |
|---|---|---|---|---|---|---|---|---|---|---|---|---|---|---|---|---|---|---|
| **SAR11 Sub-group** | **Number of Genomes** | | **1** | **2** | **3** | **4** | **5** | **6** | **8** | **9** | **10** | **11** | **12** | **13** | **14** | **15** | **16** | **18** |
| | | | | | | | | | | | | | | | | | | |
| V | 1 | | 1 | 1 | 1 | 0 | 0 | 0 | 0 | 0 | 0 | 0 | 0 | 0 | 0 | 0 | 0 | 1 |
| III | 2 | | 0 | 0 | 0 | 2 | 2 | 2 | 2 | 2 | 0 | 0 | 0 | 0 | 0 | 0 | 1 | 2 |
| II | 1 | | 1 | 1 | 0 | 0 | 1 | 1 | 1 | 1 | 0 | 0 | 0 | 0 | 0 | 0 | 1 | 1 |
| IA.1/IA.2 | 8 | | 0 | 0 | 0 | 8 | 8 | 8 | 8 | 8 | 8 | 8 | 8 | 8 | 8 | 8 | 8 | 0 |
| IA.3 | 4 | | 0 | 0 | 0 | 4 | 4 | 4 | 4 | 0 | 4 | 0 | 0 | 0 | 0 | 0 | 4 | 3 |

***Enzyme names (see Fig. S4)**:* 1 – 6-phosphofructokinase, 2 – pyruvate kinase, 3 – pyruvate carboxylase, 4 – phosphoenolpyruvate carboxylase, 5 – phosphoenolpyruvate synthase, 6 – malic enzyme, 8 – malate synthase, 9 – glycolate oxidase, 10 – isocitrate lyase, 11[a] – glucose dehydrogenase, 12[a] – gluconolactonase, 13[a] - repressor, ORF, kinase (ORK), 14[a] – 6-phosphogluconate dehydratase, 15[a] – glucose/ribitol dehydrogenase, 16[a] – fumarylacetoacetate hydrolase, 18 – catalase (KatG).

***Notes**:* [a] Genes postulated to be involved in an Entner-Doudoroff glycolytic variant pathway [1].

1. Schwalbach M.S, Tripp HJ, Steindler L, Smith DP, Giovannoni SJ (2010) The presence of the glycolysis operon in SAR11 genomes is positively correlated with ocean productivity. *Environ Microbiol* 12(2):490-500.